2-1-1985

Report on Solar Energy Conversion Through the Interaction of Plasmons with Tunnel Junctions

R. J. Schwartz
Purdue University

S. Datta
Purdue University

P. E. Welsh
Purdue University

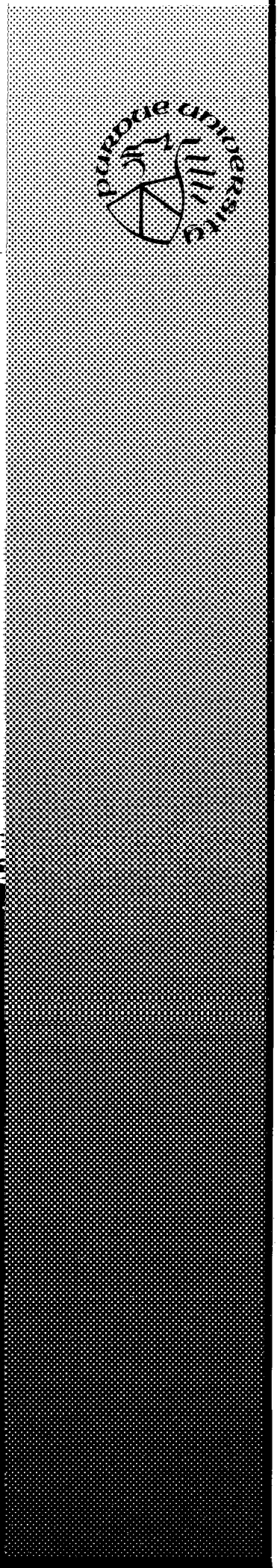

Report on Solar Energy Conversion Through the Interaction of Plasmons with Tunnel Junctions

R. J. Schwartz
S. Datta
P. E. Welsh

TR-EE 85-9
February 1985

School of Electrical Engineering
Purdue University
West Lafayette, Indiana 47907

This work was supported under grant NAG 3-433.

Report on

Solar Energy Conversion Through the Interaction of Plasmons with Tunnel Junctions

By
R. J. Schwartz
S. Datta
P. E. Welsh

School of Electrical Engineering
Purdue University
West Lafayette, IN 47907

TR-EE 85-9

February 1985

This work was supported under grant NAG 3-433.

TABLE OF CONTENTS

LIST OF TABLES

LIST OF FIGURES

Solar Energy Conversion Through the Interaction of Plasmons with Tunnel Junctions

1. Introduction

This report covers the work performed under grant NAG 3-433, "Solar Energy Conversion Through the Interaction of Plasmons with Tunnel Junctions," during the period from June 1, 1983 to December 31, 1984.

Personnel performing the work were Prof. R. J. Schwartz, Prof. S. Datta and Graduate Research Assistant P. E. Welsh. Much of the detail of the work described in this report is covered in a Master's Thesis submitted by P. E. Welsh to the School of Electrical Engineering, Purdue University, December 1984.

1.1 Limitations to Conventional Solar Cell Efficiency

A conventional pn junction solar cell is severely limited in its conversion efficiency, even under the most ideal of situations. The two major limitations, inherent in a single junction conventional solar cell, are the loss of all energy contained in the solar spectrum below the bandgap energy and the loss of photon energy in excess of the bandgap for that portion of the solar spectrum which lies above the bandgap. There are other efficiency limiting features in a conventional pn junction solar cell, but they are rather modest in comparison with the two mentioned here.

It has been known for many years that one can circumvent, at least in theory, the above problems by cascading solar cells of different bandgaps. It's not within the scope of this discussion to describe the many ways that have been proposed for accomplishing this; however, to date, none of these techniques have proved to be feasible for space application.

While the issue of solar array efficiency has always been important, it is particularly so in the case of the Space Station since the large power requirements of the Space Station translate into very large solar arrays. This in turn leads to increased drag and additional fuel for orbit maintenance. Since increases in operating efficiency translate directly into decreases in array size and drag, it's even more important now to investigate new concepts for high efficiency solar energy conversion.

This project is intended to examine a proposal first put forward by Anderson[1-3] for a conversion scheme to more effectively utilize the full solar spectrum. The

---

1. L. M. Anderson, Proceedings 17th Intersociety Energy Conversion Engineering Conference, (1982) pp. 125-130.
2. L. M. Anderson, Proceedings 16th I.E.E.E. Photovoltaic Specialists Conference, (1982), pp. 371-377.
3. L. M. Anderson, "Harnessing Surface Plasmons for Solar Energy Conversion," *Proceedings of the SPIE - The International Society for Optical Engineering*, **408**, 1983, pp. 172-178.

fundamental concepts of this new solar energy conversion scheme are described in the next section.

1.2. System Description

In its simplest form the system consists of three parts: (a) broadband coupling of the solar spectrum into surface plasmons (in a more general case, the solar spectrum is coupled into a broadband waveguide); (b) a waveguide which transmits the energy to a detector and (c) a detector which converts the optical frequency EM wave into dc electrical energy. In the case considered here the detector consists of a tunnel diode or an array of tunnel diodes.

Each of the three parts of the system can take on many forms. The wideband coupling of the solar spectrum to the guided EM wave can be accomplished by means of a prism, a grating, or perhaps, even by means of a roughened metallic surface. The structure which guides the EM wave to the detector can take the form of a 2, 3, 4, or 5 layer (and perhaps even more) thin film waveguide. The detector may be a conventional solar cell brought in close proximity to the waveguide such that fringing fields couple into the solar cell, (see Fig. 1.1) or it may take on any one of the number of forms of tunnel diodes (see Fig. 1.2).

1.3. Purpose and Scope of this Study

The purpose of this work is to:

1. Understand the critical parameters involved in this energy conversion scheme.
2. Develop a design which is capable of utilizing the inherent high conversion efficiencies of such a scheme.
3. Demonstrate the feasibility of the guided wave-tunnel detector energy conversion system.

Since portions of this system are under study by various other organizations, the scope of this investigation has been limited in the following way: Problems associated with coupling the solar spectrum into surface plasmons or other guided EM waves are not considered. Likewise a detection scheme which utilizes a conventional solar cell coupled into the fringing field of the guided wave is excluded. The primary emphasis of this study is on the waveguide and the detector portions of the system. Tunnel structures are considered as the primary detection scheme.

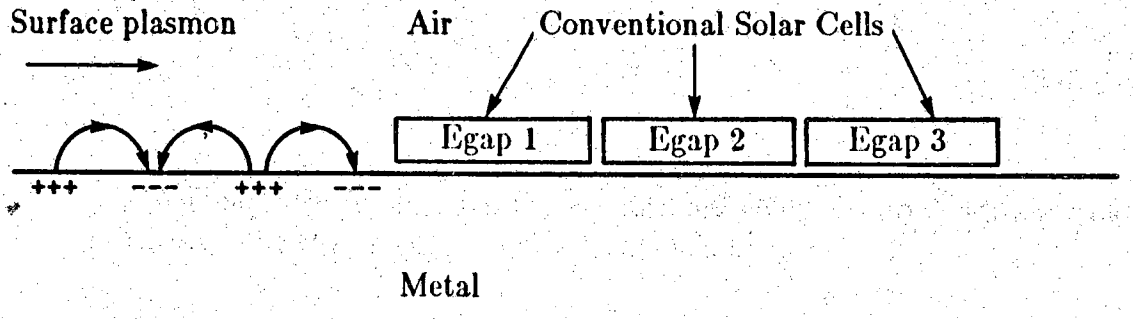

Figure 1.1. The fringing field of the surface plasmons are coupled into a series of conventional cells with progressively smaller bandgaps.

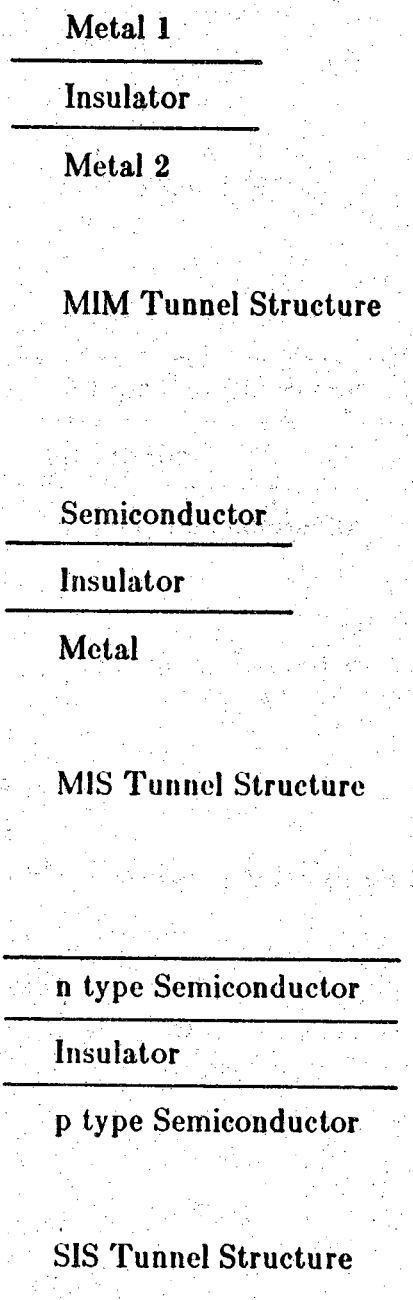

Figure 1.2. Possible tunnel structures to be considered in this report.

1.4 Summary of the Results

A sequential tunnel structure has been conceived which, if proper materials can be found, will be capable of broadband conversion of the solar spectrum without the need for spectral splitting.

Three, four and five layer transmission structures have been examined in detail with the following results:

a. Low attenuation modes were found in all cases.

b. Those structures which support modes which can cause tunneling are only weakly coupled.

c. Structures which are most strongly coupled have very short propagation distances.

d. Transmission and tunnel structures composed of semiconductors rather than metals may give acceptable results.

e. Stacked tunnel structures may be required to raise the coupling of electromagnetic waves to tunneling to acceptable levels.

The primary barrier to implementation of this energy conversion scheme appears, at this time, to be the weak coupling between the EM wave and the induced tunneling. Possible solutions to this problem have been identified and will be pursued under future work.

2. System Considerations

2.1. System Requirements on the Transmission Path

The length of the transmission path from the point of optical coupling to the detector may be quite large. Therefore, the transmission loss associated with the waveguide portion of the device should be kept as low as possible. The attenuation in the transmission link is a function of the waveguide structure and the mode which is used to propagate the energy. Each of the waveguide structures studied had at least one mode with a low attenuation coefficient. The system requires that the mode which is propagated be one which efficiently couples energy into the tunnel detector, or that efficient mode conversion between a low attenuation mode, with weak coupling, and a mode with strong coupling be possible.

It has been shown that in a two layer structure, consisting of air and silver, efficient coupling between the solar spectrum and a surface plasmon mode is possible[1]. In addition, the surface plasmon mode propagates with low attenuation. However, the surface plasmon mode does not couple well into a tunnel structure. This means that the surface plasmon mode would need to be converted to a mode with strong coupling to the tunnel structure. Such mode conversion in all likelihood, would lead to reflection of energy. In addition, the strong coupled mode would have to have a sufficiently low propagation attenuation coefficient so that most of the energy would be absorbed by tunneling in the detector.

2.2 System Requirements on the Detector

The dimension of the tunnel detector in the direction of propagation of the EM wave may be many times the optical wavelength. Therefore, the detector structure cannot be treated as a lumped device, but in fact, needs to be treated as a distributed device. This means that the analysis of the detector portion of the system will proceed as though it too were a transmission line with the mechanism of tunneling occurring in addition to transmission losses. Efficient energy conversion requires that attenuation of the EM wave due to the transfer of energy in the tunneling process be much larger than the attenuation due to losses through energy dissipation in the conductors and dielectric. If this is not the case, an excessive amount of energy is dissipated as heat and is not available for conversion to electrical energy.

The tunnel detector, like the conventional solar cell, can be viewed as having a dark current which flows under the forward bias conditions which prevail when the cell

---

1. T. K. Gustafson, "Coherent Conversion of the Sunlight Spectrum," NASA Grant NAG 3-88, (July 1980 - April 1982), Chapter III.

is in operation. The dark current is linearly dependent on the area of the detector, and hence, on the dimension of the detector in the direction of the EM propagation. It is important to keep the dimension of the detector in the direction of propagation as small as possible. The minimum dimension will be set by the attenuation of the EM wave due to tunneling. Thus, it is highly desirable to have the absorption coefficient due to tunneling as large as possible.

The dark current, which can take the form of reverse tunneling or in some cases, current injected over the tunnel barrier, serves the same role in limiting tunnel diode performance as it does in the case of the conventional solar cell. We will discuss this in more detail in section 4.1.

If the proposed energy conversion scheme is to have high efficiency, of course, it is necessary that the detector be capable of efficiently transforming the energy in the EM wave to dc energy over the full solar spectrum. That is, the detector must be tunable to a wide range of EM frequencies. The tunnel detectors have this inherent property, which is, of course, what makes them so attractive. The mechanisms which allow this to occur are discussed in section 4.1, where we describe the details of the tunnel detector operation.

2.3 Summary of the System Requirements

In order for the system to be an efficient converter of solar energy to dc electrical energy, one must have efficient conversion of the solar spectrum into a guided EM wave over the entire spectrum. The guided EM wave must have low attenuation losses and must either be capable of being coupled directly into a tunnel structure or must be capable of being efficiently converted to a mode which has a strong coupling coefficient in the tunnel structure. The tunnel detector must have the property that a large fraction of the energy in the EM wave is transferred to carriers which tunnel through the barrier, with a small percentage of the energy being absorbed as heat. In addition, the absorption coefficient due to tunneling must be as large as possible in order to reduce the effects of dark current.

In the next section we will investigate the propagation characteristics of a number of waveguide structures. The purpose of this investigation will be to determine the absorption coefficient of these structures and the dependence of this absorption coefficient on frequency, materials parameters, structure, and device dimensions. In addition, information obtained on these waveguide structures will be applied directly to the analysis of the performance of the tunnel detectors which is taken up in section 4.

3. Waveguide Propagation Studies

3.1 Introduction

In this section we will analyze three, four and five layer waveguide structures. Each of these structures will be shown to have at least one mode with a very long propagation distance, suitable for meeting the requirement of low loss propagation in the waveguide. The surface plasmon mode of the two layer structure has also been shown to be efficiently coupled to the solar spectrum. However, a two layer structure is not appropriate for a tunnel device, nor is the surface plasmon mode capable of coupling strongly into such a tunnel structure. We will see, in our analysis of the four layer structure, that it too has a mode with a very long propagation distance. In addition, a four layer structure can be constructed with a tunnel region capable of performing the desired energy conversion. As we shall see, the mode of interest is easily visualized as a perturbation of the surface plasmon mode and the four layer structure may be viewed as a perturbation of the two layer structure.

Our first concern will be for a calculation of the attenuation coefficient associated with the various modes which will propagate on each of the structures. As we have seen in section 2, one requirement is for very low attenuation. We will also be interested in which modes propagate, as we will need to find modes capable of supporting a strong electric field across a thin insulating region in order to obtain tunneling in the detector portion of the structure. Further investigation of the modes which propagate in the various structures will give us information about the possibility of mode conversion as discussed in section 2.

As mentioned previously, the two layer structure is of interest because of the low attenuation surface plasmon mode which will propagate on this structure, and because it can be efficiently coupled to the solar spectrum. The three layer structure is analyzed in two forms: A oxide-metal-oxide structure, which is of interest, because of its very long propagation distances and a metal-oxide-metal structure because it forms the simplest tunnel diode configuration. The four layer structure is of interest because it simultaneously allows for the propagation of modes with very low attenuation coefficients and has the potential for fabrication in a form suitable for a tunnel detector. The five layer structure is of interest for the same reasons as the four layer structure, with the additional attribute, that it allows us to check our results with those published by Stegeman and Burke[1]. The agreement with Stegeman and Burke's results is found to be excellent.

---

1. G. I. Stegeman and J. J. Burke, "Long Range Surface Plasmons in Electrode Structures," *Applied Physics Letters*, **43**, no. 3 (1 August, 1983), pp. 222-223.

3.2 Technique for Obtaining Attenuation Coefficients

In this section we will describe the technique used to analyze the propagation of EM waves in the various waveguides which have been considered. In this analysis the direction of propagation is the z direction and the x axis is perpendicular to the parallel planes that make up the waveguide. (See Fig. 3.1). The parallel plane waveguide fields are constant along the y direction.

3.2.1 Relation of α to k_z

For homogeneous materials,[2]

$$\nabla\cdot\bar{E}=\frac{1}{\epsilon}\nabla\cdot\bar{D}. \tag{3.1}$$

If the dielectric layers contain no charge, then $\nabla\cdot\bar{D}=0$ in those layers. In the conductive layers, $\nabla\cdot\bar{D}=0$ because no net charge exists in a conductor. From eqn (3.1), if $\nabla\cdot\bar{D}=0$, then $\nabla\cdot\bar{E}=0$. If we manipulate Maxwell's equations and use the fact that $\nabla\cdot\bar{E}=0$, it can be shown[3] that

$$\nabla^2\bar{E}=-k^2\bar{E} \tag{3.2}$$

where

$$k=\frac{2\pi}{\lambda}=\omega\sqrt{\mu\epsilon}. \tag{3.3}$$

In eqn. (3.3), λ is the wavelength, ω is the angular frequency and μ and ϵ are, respectively, the permeability and permittivity of the medium through which the wave is propagating.

A solution to the wave equation is

$$\bar{E}=\bar{E}_0e^{j(\omega t-\bar{k}\cdot\bar{r})}=\bar{E}_0e^{j\omega t}e^{-j(k_xx+k_yy+k_zz)} \tag{3.4}$$

where

$k_x\equiv$ wave number in the x direction
$k_y\equiv$ wave number in the y direction
$k_z\equiv$ wave number in the z direction.

---

2. Edward Jordan and Keith Balmain, *Electromagnetic Waves and Radiation Systems*, 2nd ed., (Englewood Cliffs, N.J.: Prentice Hall, Inc., 1968), p. 112.

3. Simon Ramo, John Whinnery and Theodore Van Duzer, *Fields and Waves in Communications Electronics* (New York: John Wiley & Sons, Inc., 1965), p. 246 and p. 372.

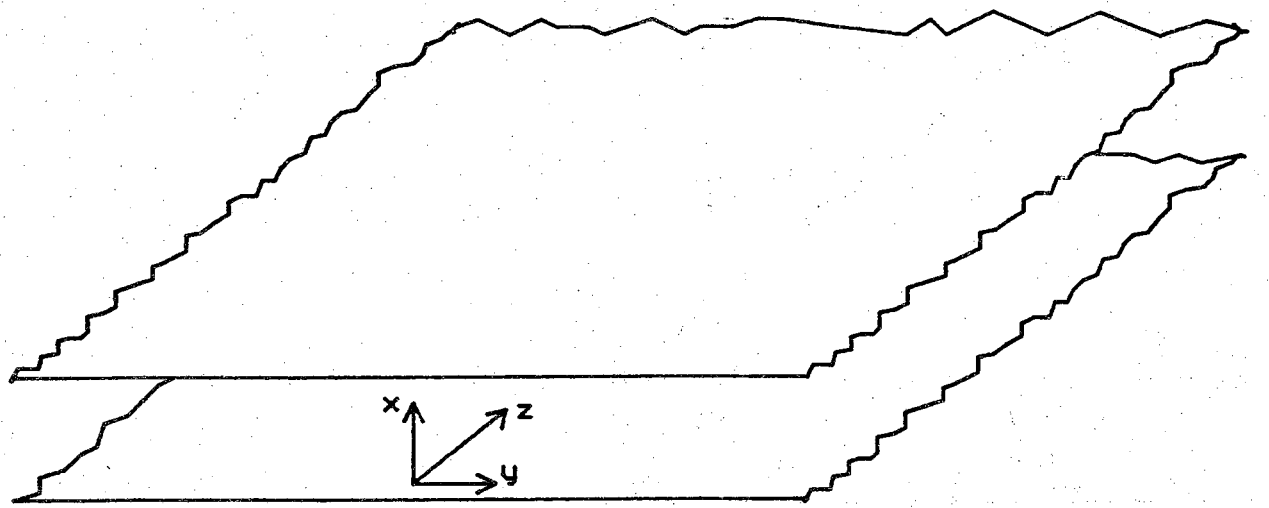

Figure 3.1. Parallel plate waveguide.

Substituting eqn. (3.4) into eqn (3.2), we obtain

$$k^2=k_x^2+k_y^2+k_z^2. \tag{3.5a}$$

For the waveguide in Fig. 3.1, the fields are constant along the y direction. Consequently, $k_y=0$, and

$$k^2=k_x^2+k_z^2. \tag{3.5b}$$

The wave propagates primarily in the z direction. The boundary conditions for Maxwell's equations require that the tangential electric and tangential magnetic fields must be continuous across all the layers in the waveguide. For this to be true, k_z must be the same in all the layers of the waveguide.[4]

k_z is a complex number and separates into real and imaginary parts.

$$k_z=\beta - j\alpha . \tag{3.6}$$

The light wave travels down the waveguide with an attenuation α. If k_z can be calculated for a waveguide, then the attenuation coefficient of the light wave is just the imaginary part of k_z.

3.2.2 Calculation of k_z

First, it needs to be shown that one of Maxwell's equations

$$\nabla\times\bar{H}=\bar{J}+j\omega\bar{D} \tag{3.7}$$

(where $\bar{J}$ is the current density and $\bar{D}$ is the electric flux density) transforms into

$$\nabla\times\bar{H}=j\omega\epsilon\bar{E}. \tag{3.8}$$

The constitutive relations state that

$$\bar{J}=\sigma\bar{E} \tag{3.9a}$$

and

$$\bar{D}=\epsilon'\bar{E} \tag{3.9b}$$

where σ is the conductivity and ϵ' is the permittivity.

From eqns. (3.9a) and (3.9b), eqn. (3.7) becomes

$$\nabla\times\bar{H}=\sigma\bar{E}+j\omega\epsilon'\bar{E}. \tag{3.10}$$

Redefining the dielectric constant simplifies eqn. (3.7). The new definition is

---

4. Ramo, Whinnery and Van Duzer, p. 359.

$$\epsilon=\epsilon'-j\frac{\sigma}{\omega} \tag{3.11}$$

and eqn. (3.10) becomes

$$\nabla\times\bar{H}=j\omega\epsilon\bar{E}. \tag{3.12}$$

For the tunnel junction solar cell, small attenuation due to propagation losses is not the only requirement. Tunneling must also be induced to extract energy. Tunneling requires a strong electric field across the thin dielectric layer. This demands that the electric field in the x direction (E_x) be non-zero. TE modes are not of interest because E_x is zero for those modes. The modes of interest are the TM modes(For a description of TE and TM modes, see Ramo, Whinnery and Van Duzer, chapter 7).

For TM modes, $E_y=H_x=H_z=0$, so eqn. (3.12) reduces to the following equations.[5]

$$E_x=\frac{k_z}{\omega\epsilon}H_y. \tag{3.13a}$$

$$E_z=\frac{-j}{\omega\epsilon}\frac{\partial H_y}{\partial x}. \tag{3.13b}$$

To find a solution for k_z, one calculates H_y and E_z as a function of x. One method assumes a plane wave solution for $H_y(x)$ (magnetic field in the y direction as a function of x).

$$H_y(x)=Ae^{jk_x x}+Be^{-jk_x x} \tag{3.14a}$$

(The $e^{j(\omega t-k_z z)}$ dependence will be assumed).

Eqn (3.13b) provides the relationship needed to find the corresponding form of E_z.

For a multi-layered waveguide, the solutions for H_y and E_z shown above are applied to every layer. For instance, the H_y field of the m^{th} layer has the form

$$H_{ym}(x)=A_m e^{jk_{xm}(x-x_m)}+B_m e^{-jk_{xm}(x-x_m)} \tag{3.14b}$$

where k_{xm} is the wave number in the x direction of the m^{th} layer and x_m is a reference point.

The fields in semi-infinite layers go to zero at large distances from the uppermost and lowermost interfaces. Consequently, if the top layer is labeled 1, then A_1 is zero

---

5. Dietrich Marcuse, *Theory of Dielectric Optical Waveguides* (New York: Academic Press, 1974), pp. 14-16.

and likewise, if the bottom layer is labeled p, then B_p is zero(See Fig. 3.2). For a solution of the four layer waveguide, see appendix A.

After the H_y and E_z fields have been found, the boundary conditions needed to obtain k_z require that H_y and E_z be continuous across the interfaces between the layers. Knowledge of the forms of the H_y and E_z fields, and their boundary conditions, is sufficient to solve the dispersion relationship. k_z is calculated from this dispersion relationship which depends upon the material parameters of each layer and the frequency of the propagating light.

3.3 Numerical Methods

Since the dispersion equation is transcendental, a computer is used to obtain k_z. The Newton Raphson method was used to solve the 3, 4 and 5 layer configurations. Appendix B describes the use of the Newton Raphson method for complex numbers.

3.4 Computation of Electric and Magnetic Fields

The E_x, E_z and H_y fields may now be determined. These fields depend on k_z. When k_z is known, the boundary conditions of the electric and magnetic fields determine the relative magnitudes of these fields. From these fields, the Poynting vector is calculated to obtain the power flow.

The solution for the H_y field is straightforward. Assume the form of the H_y field

$$H_y = A_m e^{jk_{xm}(x-x_m)} + B_m e^{-jk_{xm}(x-x_m)} \qquad (m^{th} \text{ layer}). \tag{3.15}$$

We obtain from eqn (3.5b)

$$k_{xm}^2 + k_z^2 = \omega^2 \mu_o \epsilon_m, \tag{3.16}$$

ϵ_m is the dielectric permittivity of the m^{th} layer and μ_o is the permeability of space. Eqn. (3.16) determines k_{xm} for each layer. To solve for H_y, choose a value for H_y at an interface that borders a semi-infinite layer. This will fix the values of the A_m's and B_m's of the other layers. Once all the A_m's and B_m's are known, H_y can be found at any value of x. For an example of how to calculate H_y, see Appendix C.

Since E_x and E_z are related to H_y by eqns. (3.13a) and (3.13b), $E_x(x)$ and $E_z(x)$ are calculated once $H_y(x)$ is known.

3.5 Computation of the Poynting Vector

The Poynting vector is defined for the TM mode as,

$$\bar{S} = -\bar{a}_x E_z H_y + \bar{a}_z E_x H_y. \tag{3.17}$$

$\bar{S}$ is the instantaneous power vector.

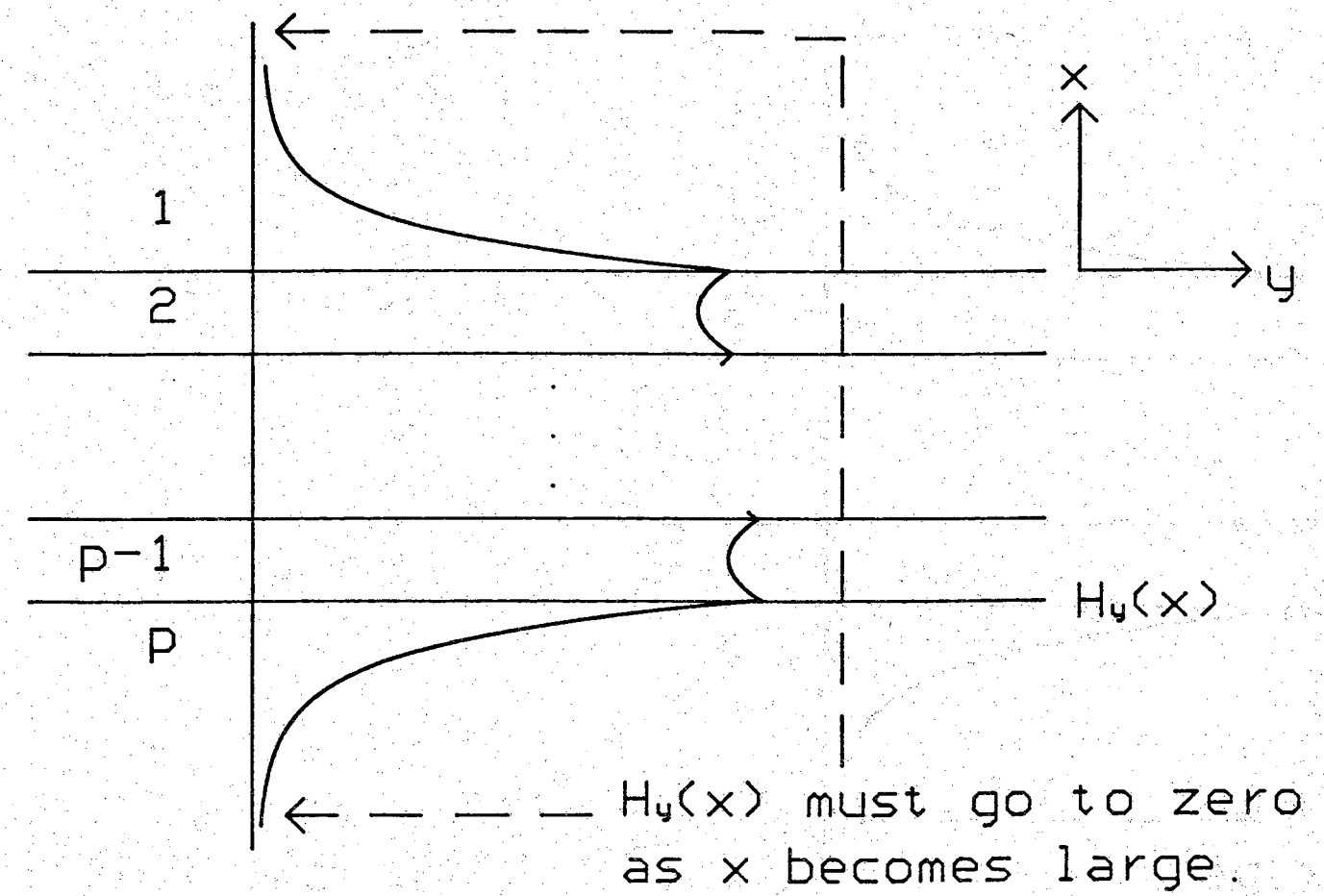

Figure 3.2. $H_y(x)$ in a p-layer waveguide.

Attenuation is due to Ohmic losses. Ohmic losses are associated with time average power lost. Consequently, the power vector of interest is the time average Poynting vector. It is defined as

$$\bar{P}=\frac{1}{2}\mathrm{Re}[\bar{E}\times\bar{H}^*] \tag{3.18}$$

where the superscript * denotes the complex conjugate value. Taking the cross product for a TM wave,

$$\bar{P}=\frac{1}{2}\mathrm{Re}[-\bar{a}_x E_z H_y^* + \bar{a}_z E_x H_y^*]. \tag{3.19}$$

Using eqn. (3.13a) and (3.13b), we obtain

$$\bar{P}=-\bar{a}_x\frac{1}{2}\mathrm{Re}[\frac{1}{j\omega\epsilon}(\frac{\partial H_y}{\partial x})H_y^*]+\bar{a}_z\mathrm{Re}[\frac{k_z}{\omega\epsilon}|H_y|^2] \tag{3.20}$$

or

$$\bar{P}=\bar{a}_x\frac{1}{2}\mathrm{Re}[\frac{j\omega\epsilon^*}{|k_z|^2}(\frac{\partial E_x}{\partial x})E_x^*]+\bar{a}_z\mathrm{Re}[\frac{\omega\epsilon}{k_z}]|E_x|^2. \tag{3.21}$$

The Poynting vector is separable into two components,

$$\bar{P}=\bar{a}_x P_x+\bar{a}_z P_z. \tag{3.22}$$

P_x represents an average power flow perpendicular to the layers. In a metal with semi-infinite width, the power lost in the metal equals P_x integrated over the area of the metal.[6]

In a metal with finite thickness, P_x integrated over the area of the metal does not necessarily equal the power lost because some of the power that flows in one side will flow out the other, but P_x does furnish us with an estimate of the lost power.

P_z is the time average power flow in the direction of propagation. P_z integrated over the area perpendicular to the z direction equals the power transmitted along the waveguide.

---

6. Jordan and Balmain, p. 173.

3.6 Calculation of Attenuation from the Field Distribution

This section introduces a method for finding an approximate value of the attenuation. This approximate attenuation depends directly upon the power distribution in the waveguide. The approximate attenuation is of the form,[7]

$$\alpha_{ap}=\frac{W_x}{2W_{Td}} \tag{3.23}$$

where

$$W_{Td}=\int P_z(\text{dielectric layers})dx. \tag{3.24}$$

W_{Td} is the time average Poynting vector in the z direction integrated over the x direction in only the lossless (dielectric) regions. It does not include W_{Tc} (P_z integrated over the x direction in the conductive layers). Therefore, $W_{Td}\Delta y$ is the power flowing in the z direction through dielectric layers of a section of the parallel plate waveguide with a width Δy.

Many of the low loss waveguides examined have W_{Td} concentrated in one lossless layer which is adjacent only to metallic layers.

If the lossless layer which contains W_{Td} is a semi-infinite layer, then W_x equals the value of P_x at the interface between the metallic layer and the lossless layer. If the lossless layer which contains W_{Td} is bounded on both sides by metallic layers, then W_x is the sum of the two values of P_x at the two interfaces. Therefore, W_x equals the portion of $W_{Td}\Delta y$ that flows into the lossy region divided by the area through which it flows.

This approximation must be used with prudence. The results presented below are obtained for waveguides with perfect dielectrics and conductive materials such as silver, so α_{ap} is accurate. But α_{ap} may not be accurate if some layers are poor dielectrics or poor conductors.

The remainder of this section is devoted to the derivation of eqn. (3.23). The simplest waveguide will suffice as an example. Consider the two layer parallel plate waveguide of Fig. 3.3. One layer is perfectly lossless and the other is a good conductor.

In Fig. 3.3, this two layer waveguide is labeled with axes and power flow in and out of planes in the dielectric. $W_{Td}\Delta y$ is the power in the dielectric region flowing through the plane at $z=z_0$.

---

7. Ramo Whinnery and Van Duzer, p. 405.

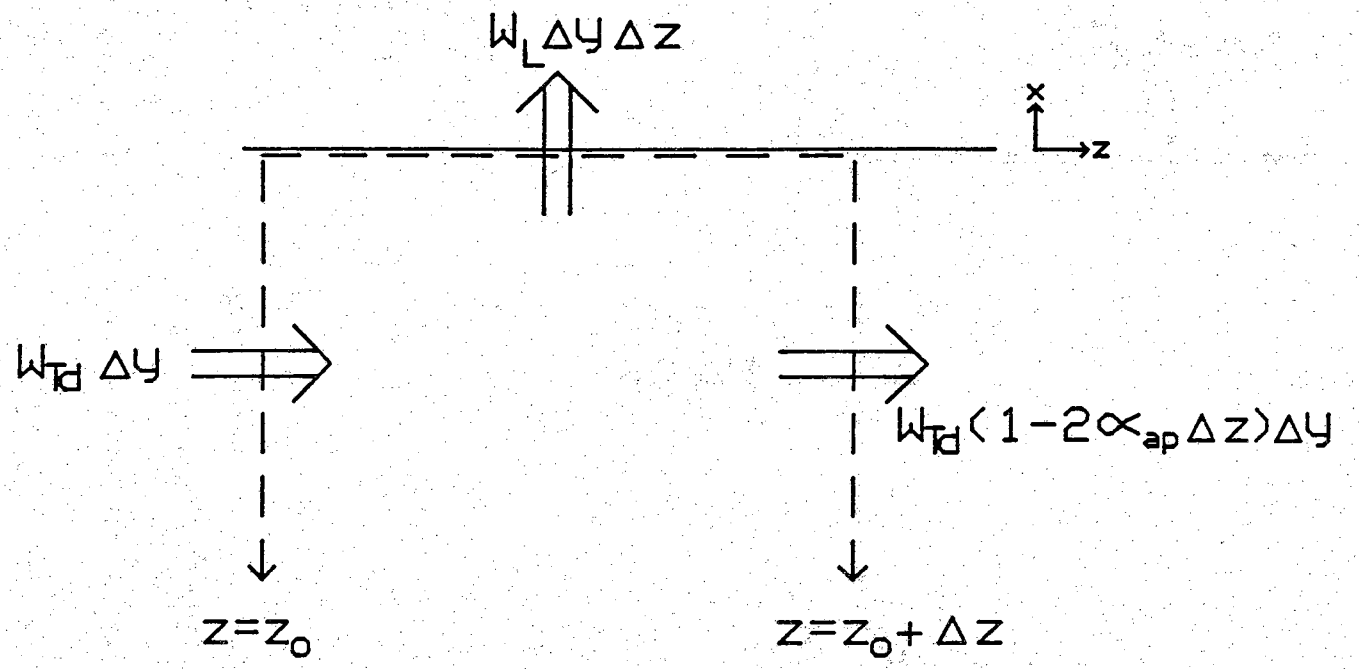

Figure 3.3. The two layer waveguide used to derive α_{ap}.

Now when eqns. (3.14a) and (3.20) are combined, the power $W_{Td}\Delta y$ is proportional to $e^{-2\alpha z}$. The power lost in the distance Δz can be approximated by

$$\frac{dW_{Td}}{dz}\Delta z = -2\alpha_{ap}W_{Td}\Delta z. \tag{3.25}$$

Consequently, $W_{Td}\Delta y(1-2\alpha_{ap}\Delta z)$ is power in the dielectric region flowing through the plane at $z=z_0+\Delta z$.

$W_x\Delta y\Delta z$ is the power flowing out of the dielectric region into the conductor. This approximately equals the power lost in the distance Δz.[8]

Setting the power lost in the dielectric in the z direction equal to the power flowing into the conductor, we get

$$W_{Td}\Delta y 2\alpha_{ap}\Delta z = W_x\Delta y\Delta z\ . \tag{3.26}$$

Solving for α_{ap},

$$\alpha_{ap} = \frac{W_x}{2W_{Td}}\ . \tag{3.27}$$

We will show that α_{ap} compares favorably with the exact attenuation obtained from the disperion relationship.

The method used to obtain the approximate attenuation utilizes a simplified form of the real part of the complex version of the Poynting Theorem.[9] This simplification is viable if α is small, i.e., if $P_z \gg P_x$.

3.7 Two Layer Structures

The two layer structure which supports the surface plasmon mode has been adequately studied by others and is not reproduced here. Very long propagation distances are obtained[10–11].

---

8. Jordan and Balmain, p. 173.
9. Johnk, *Engineering Electromagnetic Fields and Waves,* (New York: John Wiley & Sons, Inc., 1965), pp. 417-422.
10. T. K. Gustafson, "Coherent Conversion of the Sunlight Spectrum," NASA Grant NAG-3-88, (July, 1980 - April, 1982), Chapter III.
11. J. Schoenwald, E. Burstein and J. M. Elson, "Propagation of Surface Polaritons over Macroscopic Distances at Optical Frequencies," *Solid State Communications,* **12**, no. 3 (1973), pp. 185-189.

3.8 Three Layer Structures

Two three layer structures were studied, a structure consisting of oxide-metal-oxide where the metal is a thin metal layer, and a structure consisting of a metal-oxide-metal in which the oxide layer is thin. The first of these is of interest because of the long propagation distances which can be obtained with this structure. The second is of interest because it is the simplest form of a tunnel diode that can be constructed. It can give us information on the modes of propagation and strength of the electric field in the tunneling region.

3.8.1 The Oxide-Metal-Oxide Waveguide

The first waveguide we will consider is the symmetric oxide-metal-oxide(OMO) structure, where both oxides are the same material (In Fig. 3.4, $n_1=n_3=n_{oxide}$).

This OMO waveguide cannot be used in the proposed solar cell because no tunneling exists from one layer to another. However, this waveguide is considered here because it provides insight into which materials may be acceptable in the waveguide structure.

Figure 3.5 shows α_{norm} for both the TM_0 mode and the TM_1 mode for this structure.

$$\alpha = \alpha_{norm} \frac{\omega}{c} \tag{3.28}$$

We see from Fig. 3.5 that as the width of the metal is reduced, the wave will propagate farther for the TM_0 mode. If the TM_1 mode is present, the wave will attenuate much faster as the thickness of the metal decreases.

Since our primary interest is in low loss modes we will focus our attention on the TM_0 mode.

In table 3.1, we show the dependence of α on frequency in a symmetric oxide-silver-oxide waveguide. In these calculations we chose $n_1=n_3=1.5$. n_2, the index of refraction of silver, is from Johnson and Christy's paper[12]. The attenuation increases as the frequency increases.

In table 3.2, the index of refraction of the oxide layers (n_1,n_3) is varied in a symmetric oxide-silver-oxide waveguide. In these calculations we have held n_2 and the frequency constant. ($n_2=.06-j4.152$ (silver), $f=4.86\times10^{14}$Hz). α increases as n_1, n_3 increase.

---

12. P.B. Johnson and R.W. Christy, "Optical Constants of the Noble Metals," *Physical Review B*, **6**, no. 12 (15 December, 1972), pp. 4370-4379.

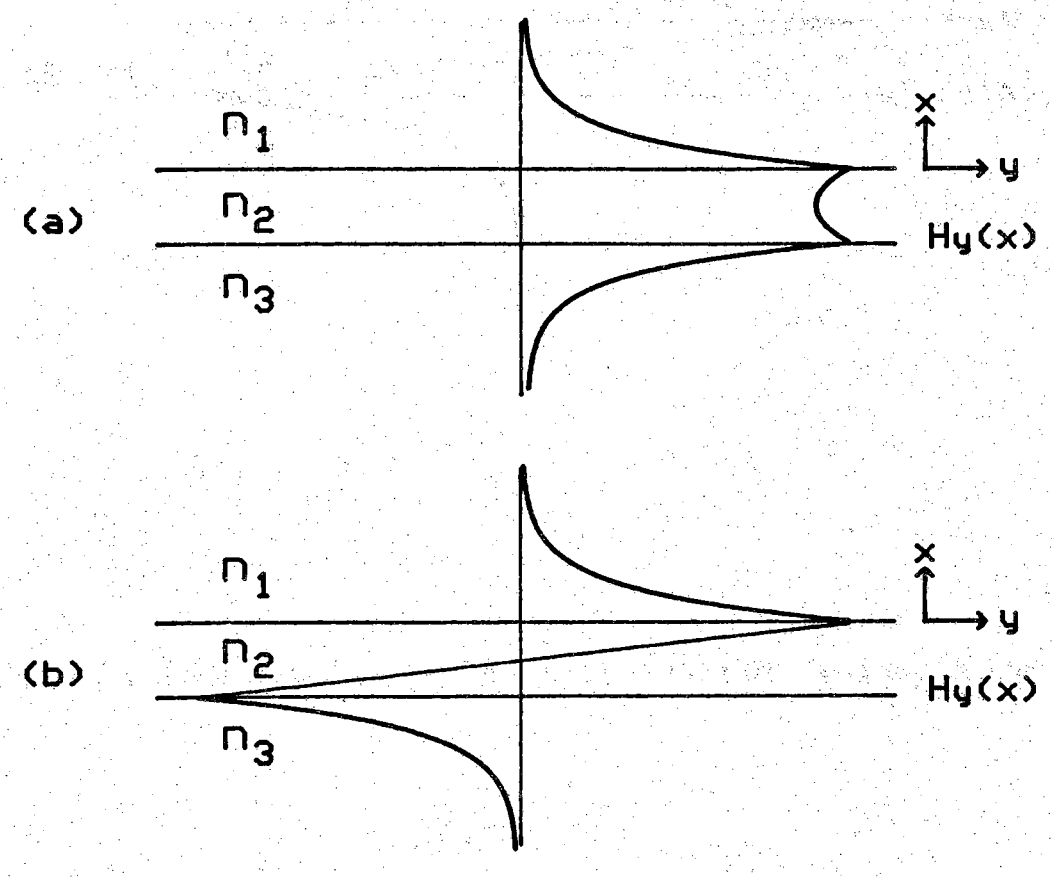

Figure 3.4. (a) TM_0 and the (b) TM_1 modes of the three layer waveguide.

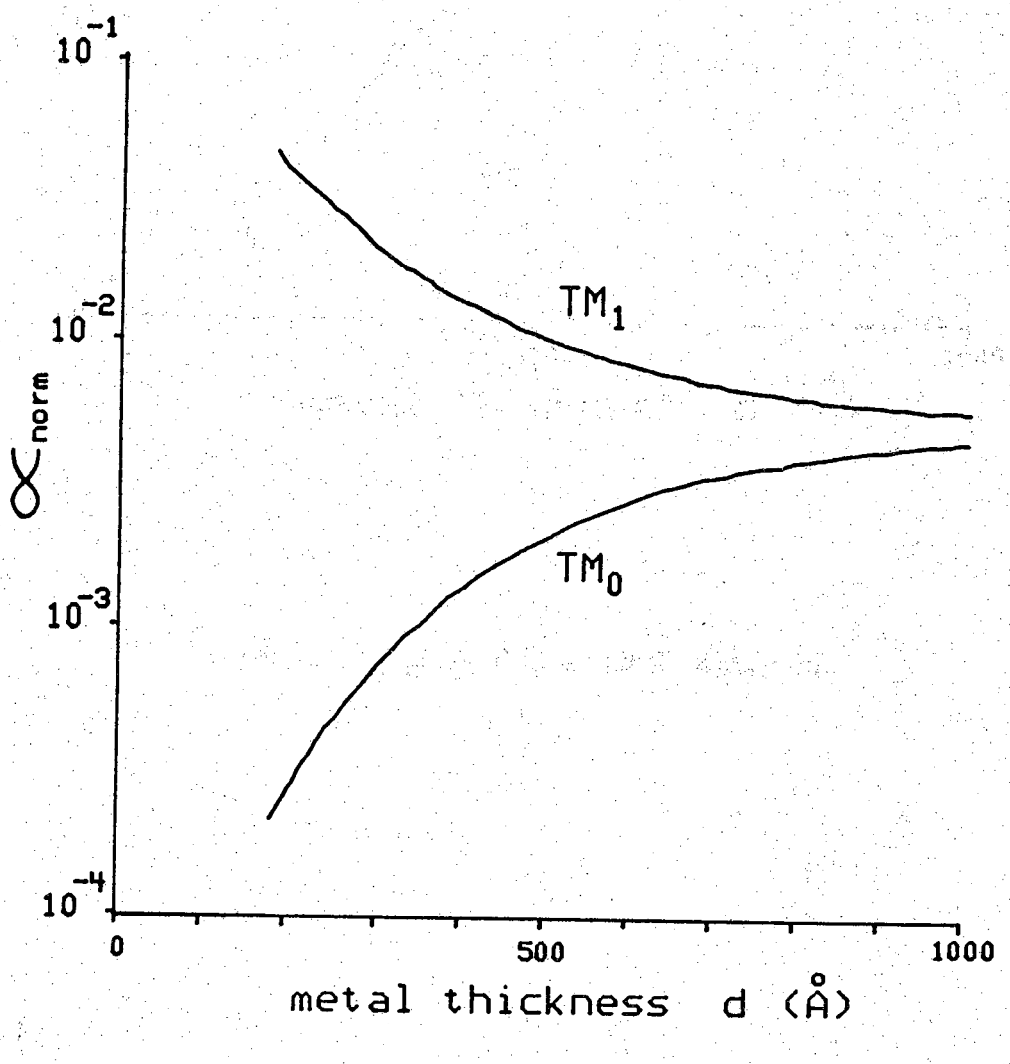

Figure 3.5. α_{norm} vs. d in an OMO waveguide.

Table 3.1
$\alpha(\text{x}10^2\text{cm}^{-1})$ in the OMO waveguide
as the frequency of light is varied.

		d(angstroms)				
freq(Hz)	n_2	180.	200.	300.	400.	500.
426.x10^{14}	.04 -j4.838	.046	.060	.16	.32	.49
486.x10^{14}	.06 -j4.152	.156	.200	.51	.97	1.49
547.x10^{14}	.06 -j3.586	.334	.422	1.06	1.93	2.92
604.x10^{14}	.05 -j3.093	.587	.741	1.80	3.24	4.82
665.x10^{14}	.04 -j2.657	1.03	1.29	3.11	5.60	8.30
725.x10^{14}	.05 -j2.275	2.93	3.69	9.07	16.7	25.1
786.x10^{14}	.05 -j1.864	8.39	10.8	30.1	64.0	108.

Table 3.2

$\alpha(\times 10^2 cm^{-1})$ in the OMO waveguide as n_1 and n_3 are varied.

	d(angstroms)				
n_1,n_3	180.	200.	300.	400.	500.
1.0	.0250	.0332	.0986	.203	.330
1.5	.155	.200	.516	.972	1.49
2.0	.647	.816	1.97	3.50	5.09
2.5	2.17	2.71	6.48	11.2	15.7
3.0	6.48	8.28	21.1	37.1	50.5
3.5	19.6	26.3	86.5	168.	213.
4.0	777.	1290.	3140.	2830.	2650.

In table 3.3, the effect of different metals are are examined while holding $n_1=n_3=1.5$ and $f=4.86\text{x}10^{14}$Hz . The indices of refraction for silver(Ag) and gold(Au) are from Johnson and Christy's paper. The indices for the other metals are listed in the Gmelin Handbuch series[13].

From table 3.3, it appears that potassium(K), rubidium(Rb), calcium(Ca) and magnesium(Mg) would work about as well as silver(Ag), for a low loss waveguide. With the possible exception of magnesium, these materials do not appear to be practical alternatives.

3.8.2 The Metal-Oxide-Metal Waveguide

The metal-oxide-metal (MOM) waveguide is made up of a thin layer of oxide sandwiched between two semi-infinite metal layers. Unlike the OMO waveguide, tunneling can occur in the MOM waveguide. Tunneling will only occur if the electric field doesn't change sign in the oxide. The only mode where this requirement is met is the TM_0 mode.

Unfortunately, as the oxide layer thickness is decreased, the attenuation increases for the TM_0 mode and the TM_1 mode. See Fig. 3.6. The region of interest for tunneling is for $d<.01$ microns.

Since we are interested in tunneling modes, tables 3.4, 3.5 and 3.6 display the attenuation of the TM_0 mode as a function of frequency, oxide index of refraction and metal type.

In table 3.4, the frequency is varied in a symmetric silver-oxide-silver waveguide. $n_1=n_3$ = index of refraction of silver. $n_2=1.0$. As the frequency increases, α increases.

In table 3.5, the index of refraction of the oxide layer (n_2) is varied. $n_1=n_3=.06-j4.152$ (silver). $f=4.86\text{x}10^{14}$Hz .

In table 3.6, the effect of different metals is examined. ($n_2=1.0$. $f=4.86\text{x}10^{14}$Hz).

From table 3.6, potassium(K), rubidium(Rb), magnesium(Mg) and calcium(Ca) would be better metals to use in the waveguides than silver(Ag) at $f=4.86\text{x}10^{14}$ Hz if the chemical problems could be overcome.

3.9 Four Layer Structures

The discussion presented in this section involves one specific type of waveguide, air-silver-oxide-silver(ASOS). The parameters needed in this section are presented in Fig. 3.7.

---

13. *Gmelin Handbuch - Der Anorganischen Chemie,* Ed. R.J. Meyer and E.H. Pietsch, (Berlin: Verlag Chemie).

Table 3.3
$\alpha(\text{x}10^2\text{cm}^{-1})$ in the OMO waveguide as n_2 is varied.

		d(angstroms)				
metal	n_2	180.	200.	300.	400.	500.
Ag	.06 -j 4.152	.156	.200	.516	.972	1.49
Au	.21 -j 3.272	1.04	1.30	3.18	5.96	9.34
Ca	.29 -j 7.94	.284	.374	.913	1.39	1.72
Cs	.326-j 4.01	.910	1.16	2.99	5.64	8.66
K	.067-j24.0	.0143	.0152	.0166	.0167	.0168
Mg	.43 -j12.0	.298	.367	.651	.790	.844
Na	.048-j 2.5	.573	.716	1.71	3.19	5.12
Rb	.135-j10.0	.110	.140	.292	.392	.442

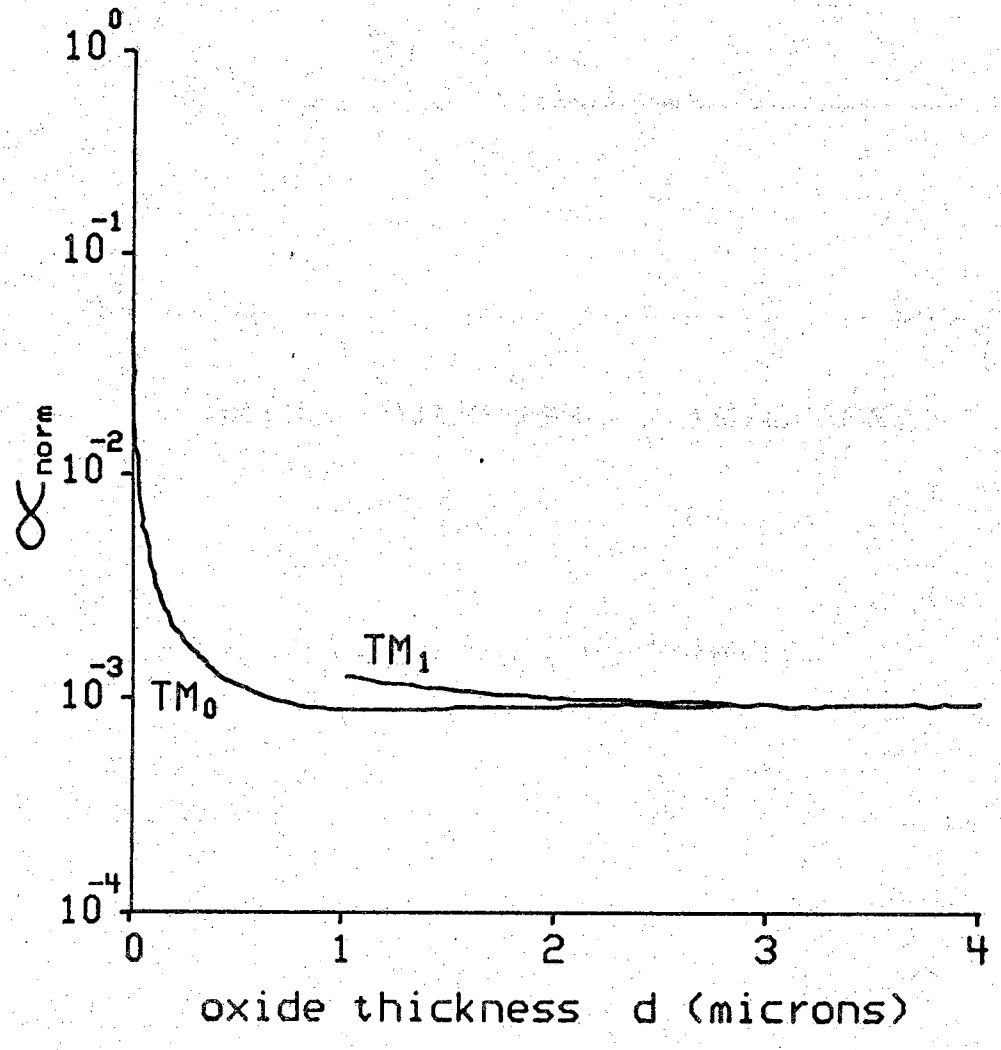

Figure 3.6. α_{norm} vs. d in an MOM waveguide.

Table 3.4
$\alpha(\text{x}10^4\text{cm}^{-1})$ in the MOM waveguide
as the frequency of light is varied.

		d(angstroms)				
freq(Hz)	n_1, n_3	10.	20.	30.	40.	50.
$426.\text{x}10^{14}$	.04 +j4.838	1.20	.522	.328	.242	.192
$486.\text{x}10^{14}$	.06 +j4.152	3.02	1.32	.815	.586	.460
$547.\text{x}10^{14}$	.06 +j3.586	4.92	2.21	1.35	.956	.738
$604.\text{x}10^{14}$	.05 +j3.093	6.60	3.06	1.89	1.33	1.02
$665.\text{x}10^{14}$	.04 +j2.657	8.55	4.08	2.58	1.82	1.39
$725.\text{x}10^{14}$	.05 +j2.275	17.5	8.52	5.48	3.97	3.05
$786.\text{x}10^{14}$	.05 +j1.864	33.6	16.6	10.9	8.02	6.29

Table 3.5
$\alpha(\times 10^4 cm^{-1})$ in the MOM waveguide as n_2 is varied.

	d(angstroms)				
n_2	10.	20.	30.	40.	50.
1.0	3.02	1.32	.815	.586	.460
1.5	7.46	3.50	2.18	1.54	1.18
2.0	14.0	6.83	4.39	3.18	2.44
2.5	24.0	11.9	7.78	5.72	4.47
3.0	41.3	20.6	13.5	10.1	7.98

Table 3.6

$\alpha(x10^4 cm^{-1})$ in the MOM waveguide as n_1 and n_3 are varied.

		d(angstroms)				
metal	n_1, n_3	10.	20.	30.	40.	50.
Ag	.06 +j 4.152	3.02	1.32	.815	.586	.460
Au	.21 +j 3.272	23.2	10.8	6.69	4.74	3.60
Ca	.29 +j 7.94	1.59	.867	.634	.514	.439
Cs	.326 +j 4.01	18.3	8.03	4.92	3.52	2.75
K	.067 +j24.0	.0394	.0261	.0203	.0168	.0145
Mg	.43 +j12.0	.868	.547	.421	.351	.303
Na	.048 +j 2.5	12.5	6.14	3.98	2.88	2.22
Rb	.135 +j10.0	.408	.244	.185	.153	.132

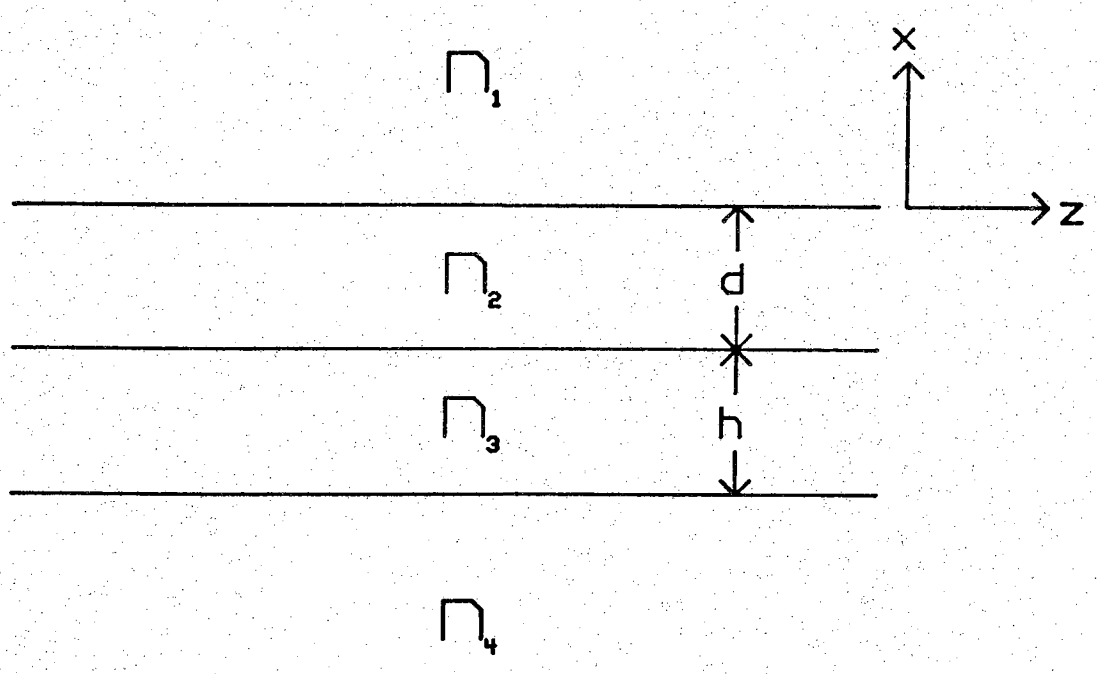

Figure 3.7. The four layer waveguide.

Two modes have been found in the ASOS waveguide. One is the TM_{10} or short range mode and one is the TM_{00} or the long range mode. The subscript 10 means that there is 1 node in the second layer and 0 nodes in the third layer. The subscript 00 means that there are no nodes in the second and third layers. Figure 3.8 displays examples of both of these modes.

If $n_1=1.0$, $n_3=1.5$, $n_2=n_4=n_{metal}=.06-j4.152$, $d=180.x10^{-10}m$, $h=10.x10^{-10}m$ and $f = 4.86 \times 10^{14}Hz$, then for the TM_{00} mode,

$$k_z=1.05x10^5-j9.47x10^1(cm^{-1})$$

and

$$\alpha=9.47x10^1(cm^{-1}).$$

Likewise, for the TM_{10} mode,

$$k_z=2.67x10^6-j7.47x10^4(cm^{-1})$$

and

$$\alpha=7.47x10^4(cm^{-1}).$$

Waves can propagate long distances in this waveguide because the propagation distance($\frac{1}{\alpha}$) of the TM_{00} mode($n_3 = 1.5$) exceeds 100 microns.

3.9.1 Perturbation of n_3 in the Four Layer Waveguide

In this section, we consider the effects of variations in the index of refraction in the thin "oxide" layer. Table 3.7 displays α and β (See eqn. (3.6).) as the index of refraction of the oxide layer varies. For table 3.7, $n_1=1.0-j0.0$; $n_2=n_4=.06-j4.152$; $d=180.x10^{-10}m$; $h=10.x10^{-10}m$ and $f=4.86x10^{14}$ Hz. All of these modes are TM_{00} modes except for

$n_3=20.-j0.$	TM_{11}
$n_3=25.-j0.$	TM_{11}
$n_3=29.-j9.8$	TM_{01}
$n_3=41.4-j9.8$	TM_{01}.

3.9.2 α_{ap} of Some Four Layer Waveguides

In section 3.6, a procedure was presented for finding an approximate value of the attenuation based upon knowledge of the electric field distribution. In table 3.8, the results of this procedure are compared to the actual attenuation for the TM_{00} mode.

For the short range T_{10} mode, when $n_1=1.0-j0.$; $n_2=n_4=.06-j4.152$; $n_3=1.5-j0.$; $d=180.x10^{-10}m$; $h=10.x10^{-10}m$ and $f=4.86x10^{14}$ Hz,

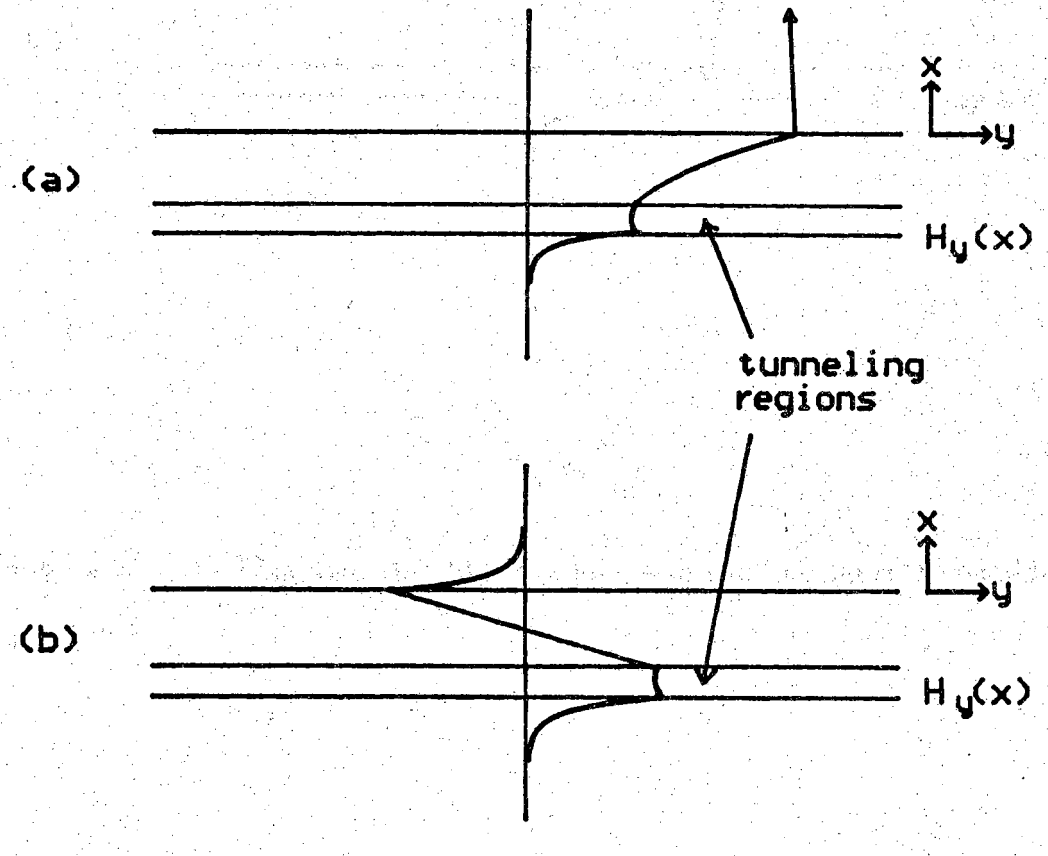

Figure 3.8. (a) TM_{00} and the (b) TM_{10} modes of the four layer waveguide.

Table 3.7
$\beta(\text{x}10^5\ \text{cm}^{-1})$ and $\alpha(\text{x}10^2\ \text{cm}^{-1})$
of the four layer waveguide.

n_3	β	α
1.5-j 0.0	1.05	.947
10.0-j 0.0	1.05	1.23
20.0-j 0.0	1.09	5.62
25.0-j 0.0	1.24	777.
1.5-j 7.5	1.05	1.46
1.5-j 9.8	1.05	1.49
16.0-j 9.8	1.05	13.1
23.2-j 9.8	1.03	21.1
29.0-j 9.8	1.02	14.2
41.4-j 9.8	1.03	3.83
1.5-j12.0	1.05	1.46
1.5-j18.0	1.04	1.26
1.5-j25.0	1.04	.958
1.5-j39.9	1.04	.533

Table 3.8
$\alpha(\text{x}10^2\ \text{cm}^{-1})$ and $\alpha_{ap}(\text{x}10^2\ \text{cm}^{-1})$
of the four layer waveguide.

n_3	W_{Td}	W_L	α	α_{ap}
1.5-j 0.0	.1533	2.898	.947	.945
10.0-j 0.0	.144	3.55	1.23	1.23
20.0-j 0.0	.1025	11.545	5.62	5.63
25.0-j 0.0	.0481	745.	777.	775.
1.5-j 7.5	.1565	4.561	1.46	1.46
1.5-j 9.8	.1592	4.731	1.49	1.49
16.0-j 9.8	.15688	41.248	13.1	13.1
23.2-j 9.8	.18143	76.545	21.1	21.1
29.0-j 9.8	.25222	71.506	14.2	14.2
41.4-j 9.8	.28636	21.978	3.83	3.84
1.5-j12.0	.1622	4.747	1.46	1.46
1.5-j18.0	.17132	4.3147	1.26	1.26
1.5-j25.0	.18195	3.4844	.958	.958
1.5-j39.9	.19935	2.1253	.533	.533

$$\alpha = 7.47 \times 10^4 (\text{cm}^{-1})$$

and

$$\alpha_{ap} = 7.46 \times 10^4 (\text{cm}^{-1}) .$$

The most obvious result from the analysis of the four layer waveguide is that α_{ap} defined in eqn (3.28) is a very good approximation.

3.10 Five Layer Structures

The five layer waveguide structure illustrated in Fig 3.9 has been analyzed and the results compared with those of Stegeman and Burke[14]. This was done to ascertain that the program used to calculate the wave number is correct for five layers.

Four modes have been studied - $TM_{000}, TM_{010}, TM_{101}$, and TM_{111}.

The fields for these modes are shown in Fig. 3.10. In Fig. 3.11, $n_1 = n_3 = n_5 = 1.5$, $n_2^2 = n_4^2 = -46. - j2.$, $d_1 = d_2 = 150.\times 10^{-10}$m, $f = 3.5 \times 10^{14}$Hz and propagation distance $= \frac{1}{2\alpha}$.

The results obtained are in agreement with those of Stegeman and Burke.

---

14. G.I. Stegeman and J.J. Burke, "Long Range Surface Plasmons in Electrode Structures," *Applied Physics Letters*, **43**, no. 3 (1 August, 1983), pp. 222-223.

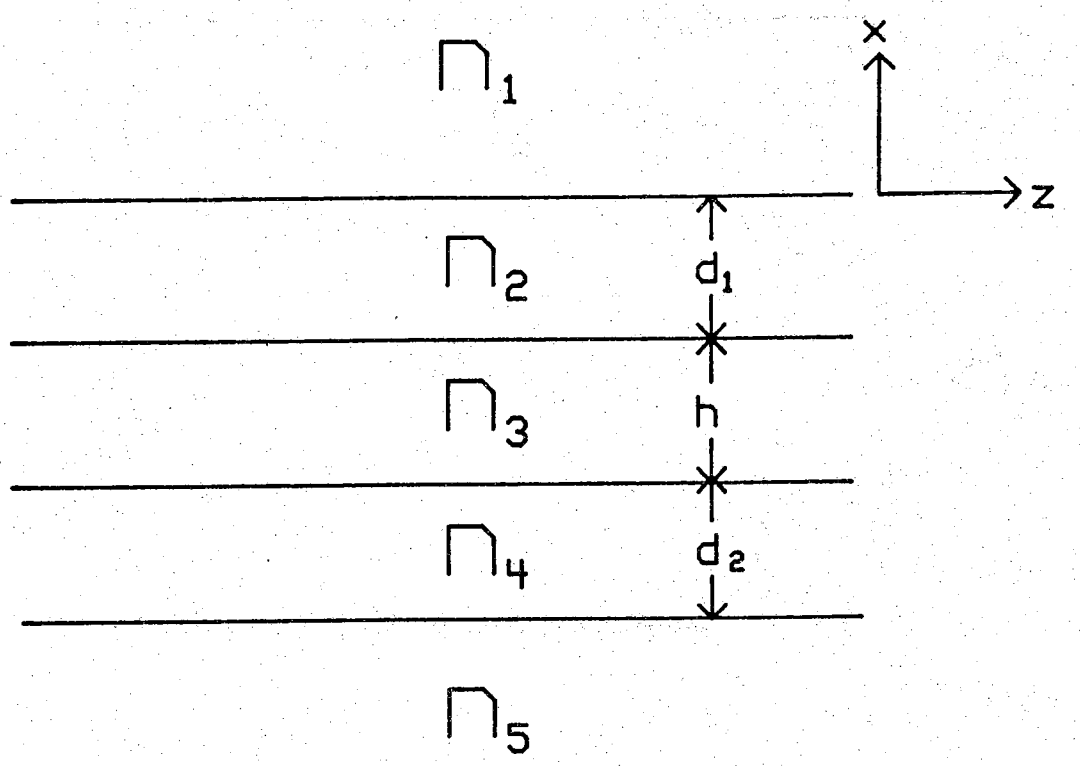

Figure 3.9. The five layer waveguide.

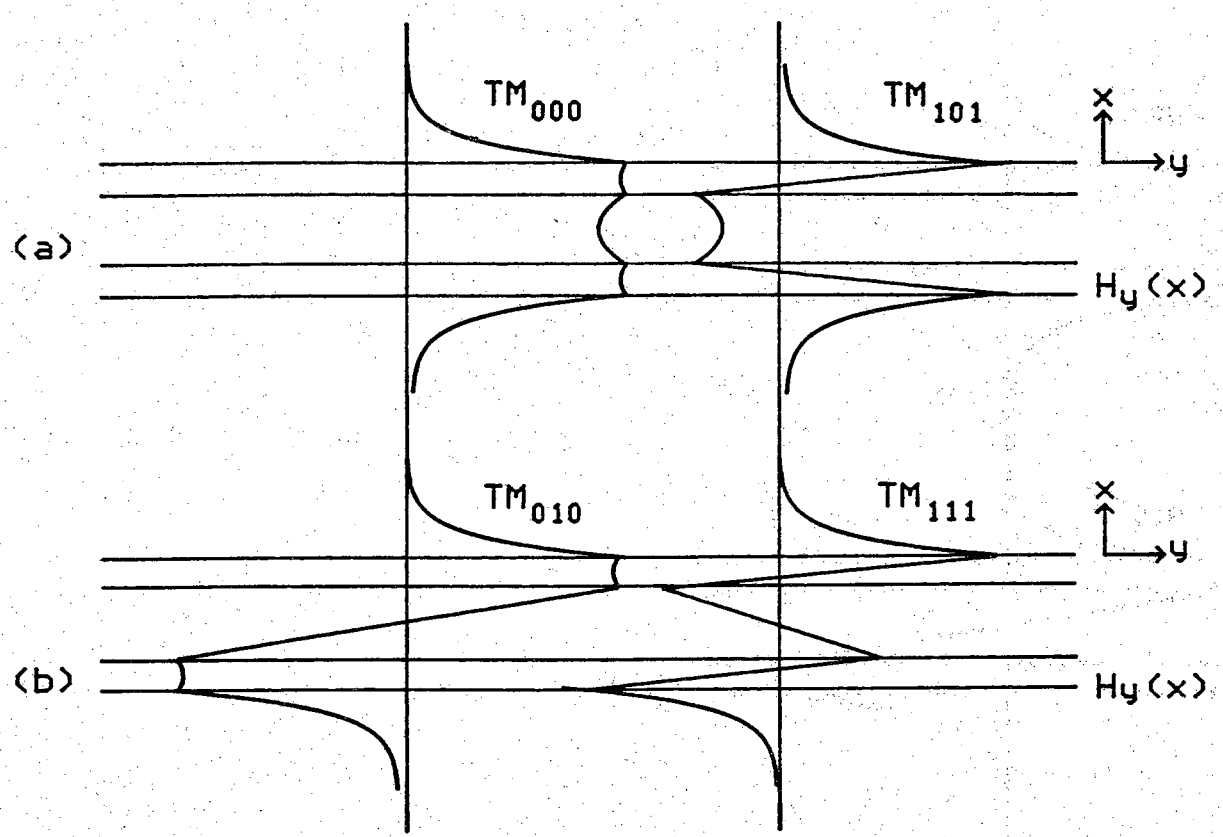

Figure 3.10. (a) TM_{000}, TM_{101} and the (b) TM_{010}, TM_{111} modes of the five layer waveguide.

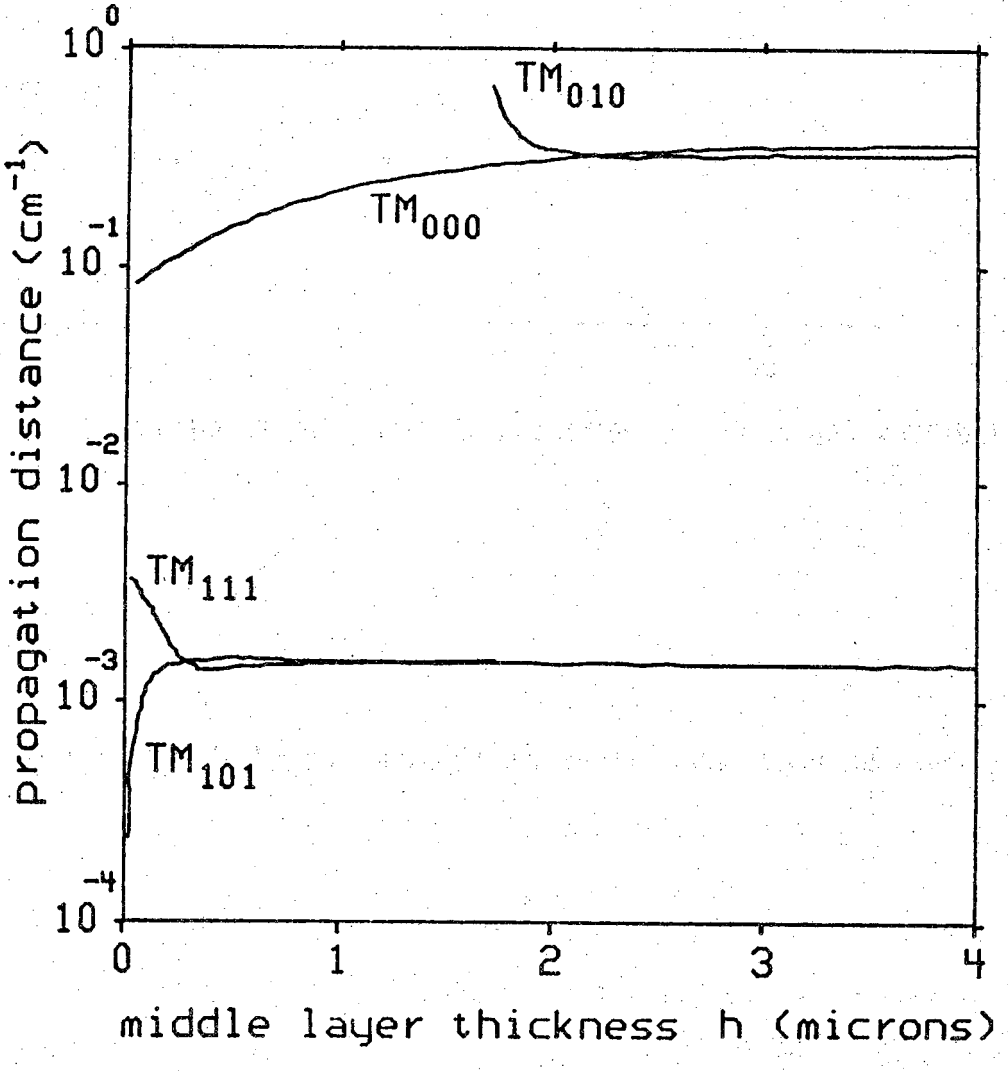

Figure 3.11. Propagation distance vs the middle layer thickness.

4. Tunnel Detector

In this section we will present a qualitative discussion of the operation of the tunnel diode detector and the various factors which impose limits on the efficient operation of this detector. We will describe various structures which have the potential for broadband detection. One of the these is a cascaded structure which is similar in concept to a cascaded multigap conventional solar cell structure. The other is a structure which in concept, is similar to a split spectrum conventional solar cell. We will present a description of the technique for estimating the absorption coefficient associated with tunneling in a distributed tunnel structure and we will present quantitative results on the strength of the coupling to a tunnel diode. Finally, we will describe a stacked tunnel diode structure which may have the potential for overcoming some of the weaknesses identified with a single tunnel diode detector.

4.1. Operation of a Tunnel Detector

In Fig. 4.1, we've shown a metal-insulator-semiconductor tunnel structure. This structure was chosen rather than a metal-insulator-metal structure since it is difficult to obtain sufficient assymmetry in the characteristics of a metal-insulator-metal tunnel diode to give useful and efficient energy conversion.

As the electromagnetic wave propagates through the tunnel diode, shown in Figure 4.1, (the direction of propagation is normal to the page) the electric field component across the insulator can result in increased tunneling through the thin insulating region. Under equilibrium conditions, the tunneling currents in the two directions are equal in magnitude and opposite in sign; however, in the presence of an electric field, the transitions of electrons from the valence band in the semiconductor to the conduction band in the metal is enhanced, since there is a large supply of occupied valence band states and a large number of unoccupied states in the metal above the Fermi level. Transitions in the other direction would be aided by the other half cycle of the electromagnetic wave; however, this does not occur (at least for photons with energy less than the energy between the Fermi level and the conduction band edge) as there are no states for the electrons from the metal to tunnel to on the semiconductor side unless the energy is greater than the energy of the conduction band edge. Thus, this asymmetric structure will allow tunneling of electrons from the valence band of the semiconductor to the metal. This, of course, will increase the potential of the metal relative to the semiconductor. In Fig. 4.2, we show the open circuit condition in the presence of sufficient photons to lift the metal potential by a voltage V_A. In this case, transitions from the valence band to the metal will require the aid of photons with energies greater than $qV_A + E_{f_p} - E_v$. In addition, tunneling in the reverse direction (from the metal into the conduction band of the semiconductor) requires photons with energy greater than $E_c - E_{f_p} - qV_A$. As the diode assumes a forward bias as a result of

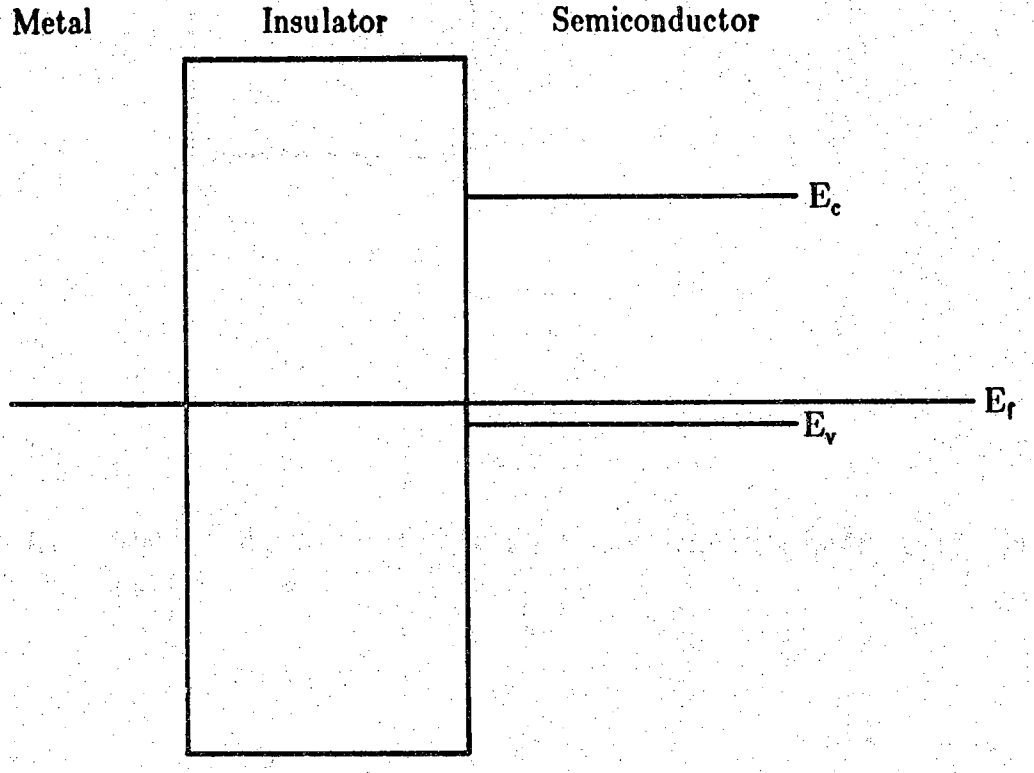

Figure 4.1. Metal insulator semiconductor tunnel structure under equilibrium conditions.

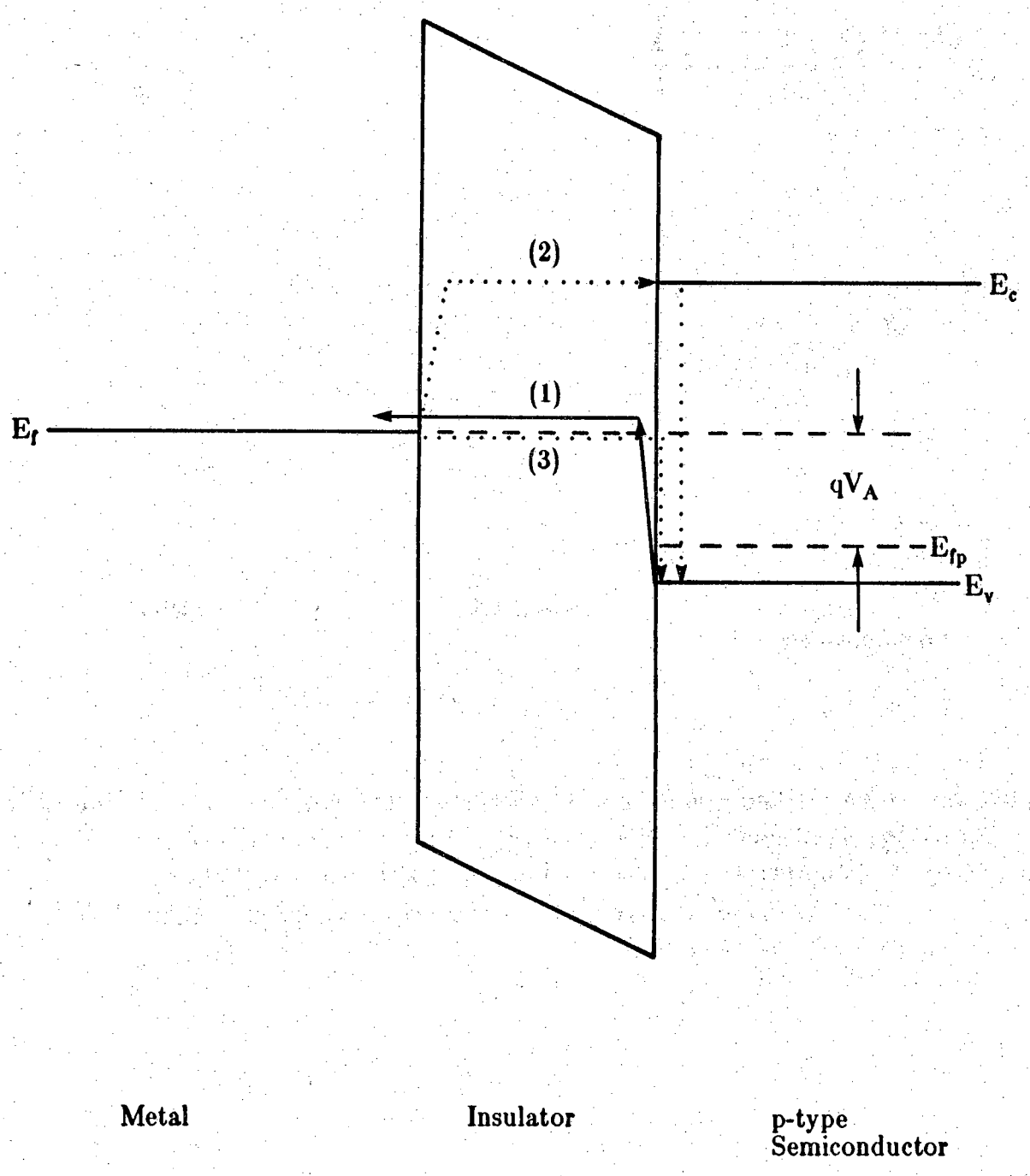

Figure 4.2. Metal insulator semiconductor tunnel structure under open circuit conditions. (1) photon aided transitions which contribute to energy conversion. (2) photon aided transitions which cause reverse current to flow (3) non-photon aided tunneling current in the reverse direction.

the conversion of the EM wave into DC electric energy, the forward tunneling is reduced, since fewer photons with sufficient energy to cause the tunneling to occur are available as compared to the zero bias case. As the forward bias on the diode builds up, the reverse tunneling process is enhanced, since as the photon energy required for reverse tunneling is reduced and the number of photons with enough energy to cause reverse tunneling is increased. In the simple ideal case, this means that when $qV_A \approx E_g/2$ the forward and reverse tunneling currents will be equal and the bias voltage on the diode will not increase further. Thus the open circuit voltage on such a device will be limited to

$$V_{oc} \approx \frac{E_g}{2q}$$

Actually the open circuit voltage will be somewhat less than this since application of a forward bias will cause dark current to flow as a result of tunneling from the metal into interfacial states at the insulator semiconductor boundary as well as do to thermionic emission over the barrier. In any event, one of the fundamental limits of a device of this sort is that the open circuit voltage will be limited to $E_g/2q$. This is in contrast to a conventional solar cell where the limit, in theory, is approximately equal to E_g/q. This may not be a serious problem, however, since the tunnel structures are majority carrier devices and one is not limited in the choice of semiconductors in the same way as in a conventional solar cell. In a conventional solar cell, the choice of semiconductor materials is limited to those with relatively long minority carrier lifetimes or in the case of short lifetime materials, those which have direct energy gaps. Such restrictions do not apply to this device. Hence the necessity for moving to wide gap materials may not be a serious problem.

It's interesting to note that the portion of the spectrum which is utilized by the tunnel diode is a function of the bias on the device. In the unbiased device nearly any photons have sufficient energy to aid in the tunneling process. As a bias develops on the cell only those photons with energy in excess of the applied bias can take part. By analogy with conventional solar cells, this is equivalent to having a material with an electronically variable band gap. This leads us to consider an interesting cascade structure.

4.2 Cascaded Tunnel Structures

The electronic tunability of a tunnel diode structure offers a unique opportunity for the broadband conversion of solar energy. Consider a cascade arrangement of tunnel structures as shown in Fig. 4.3, where the electromagnetic energy enters from the left and propagates through the structure to the right. Consider the structure initially in equilibrium with the diodes unbiased, then turn on the propagating broadband EM wave and assume for the moment that the absorption coefficient

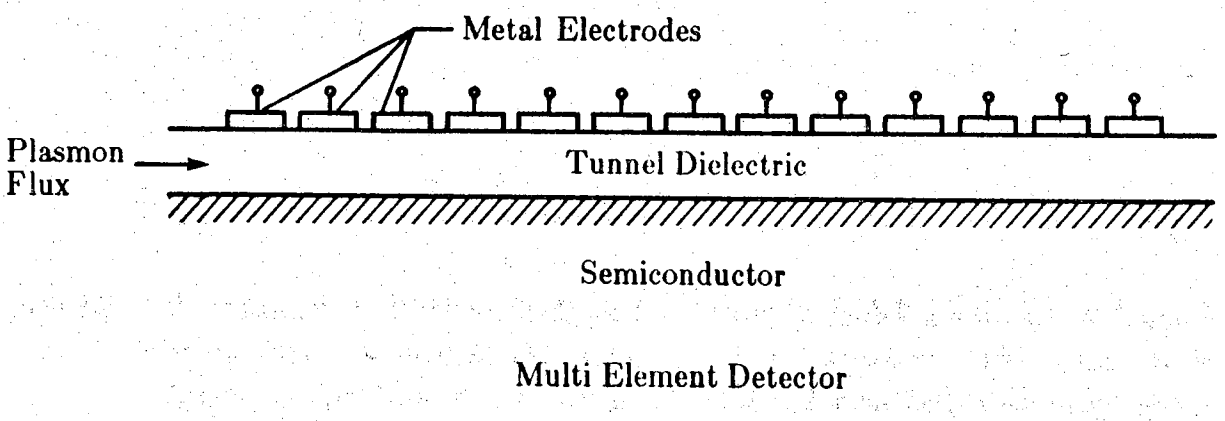

Figure 4.3. A cascaded multi-element tunnel detector in which plasmons of highest energy are absorbed at the right end of the structure. This structure is similar in operation to a stack of conventional solar cells with progressively decreasing bandgap.

associated with tunneling is very high. The propagating wave strikes the first diode on the left causing tunneling to occur. This in turn will cause the first diode to self bias to a voltage equal to $E_g/2q$, assuming there are sufficient photons in the incident wave to cause this to happen. As the bias on the diode increases, those photons in the long wavelength portion of the spectrum will no longer have sufficient energy to cause tunneling to occur. The absorption coefficient at those wavelengths will fall rapidly in the first diode. Thus, as the first diode self biases to its maximum value, the diode becomes transparent to all photons except those with energy greater than qV_{A1}. Photons not absorbed in the first diode will then propagate through the first diode and impinge on the second diode. The second diode then will self bias to a value set by the maximum photon energy which passes through the first diode. As the bias on the second diode increases, it too becomes transparent to the longest wavelength photons which then pass on through to the third diode and so on. Thus the cascade structure eventually will assume a bias on each of the diodes which is consistent with maintaining an equilibrium condition between tunneling in the forward direction due to photon aided tunnelling processes and dark current flow in the reverse direction, as discussed in the previous section. This cascade structure is the analog of a multigap stacked structure of conventional pn cells. However, it does not require multigap semiconductors. A single semiconductor energy gap is sufficient for the entire device. In Fig. 4.4, we show an embodiment of the same idea in which we use n-type and p-type tunnel diodes. This will double the voltage generated by the structures.

As shown in Figs. 4.3 and 4.4, one electrode of all the diodes is common. This presents some problems for power conditioning. It is possible that this problem can be eliminated by sectioning with isolation regions between the diodes which are small enough that they do not strongly influence the propagation of the electromagnetic wave.

4.3. Strength of Coupling Between the EM Wave and the Tunneling Process

As noted in section 2, the tunnel structure needs to be treated as a distributed system. The absorption which results from the tunneling process must be large with respect to other loss mechanisms if efficient energy conversion is to result. In this section we will discuss a technique for estimating the absorption due to tunneling.

In our calculations of attenuation due to losses during propagation down the waveguide we have assumed that the dielectric was lossless. In section 3.6 we presented a technique for the calculation of the approximate value of the attenuation coefficient based on the power flow from the dielectric region into the metal.

In that discussion, $-\frac{1}{2}\int_S \mathrm{Re}[\bar{E}\times\bar{H}^*]\cdot d\bar{S}=0$ because the volume enclosed by S was located in the lossless layer of the waveguide. Its boundaries were at $z = z_o$ and

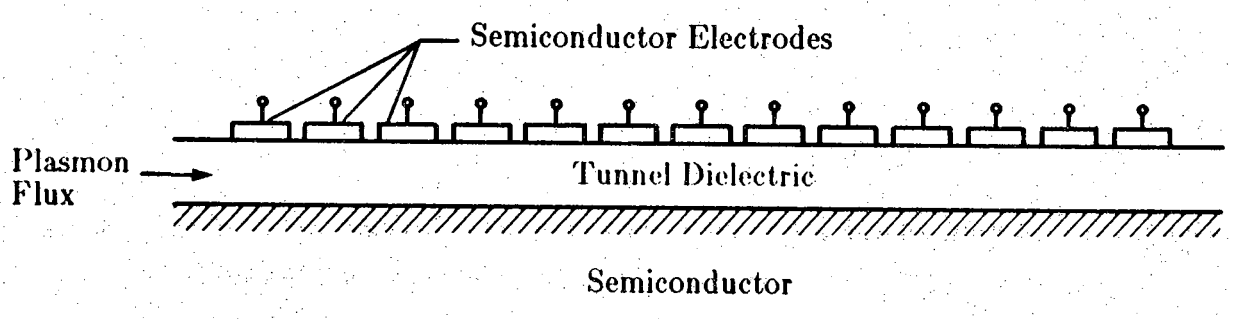

Figure 4.4. The same configuration as in Figure 4.3, with the exception that the electrodes are doped semiconductors.

$z = z_o + \Delta z$; $y = y_o$ and $y = y_o + \Delta y$ and $x = -\infty$ and $x = 0$.

In this section we will compute the attenuation due to tunneling using a similar technique. In this case however, the boundaries of the enclosed volume are located at $z = z_o$ and $z = z_o + \Delta z$; $y = y_o$ and $y = y_o + \Delta y$ and $x = -\infty$ and $x = +\infty$. Keeping this in mind, the power flowing through the plane at $z = z_o$ is $W_T \Delta y$ where

$$\int P_z(\text{all layers}) dx\, dy = \Delta y \int P_z(\text{all layers}) dx = W_T \Delta y \ . \tag{4.1a}$$

Using the same argument that produced eqn (3.25), the power flowing through the plane at $z = z_o + \Delta z$ equals $W_T \Delta y(1 - 2\alpha \Delta z)$.

In the volume specified,

$$-\frac{1}{2} \int_S \mathrm{Re}[\bar{E} \times \bar{H}^*] \cdot d\bar{S} = W_T \Delta y 2\alpha' \Delta z. \tag{4.1b}$$

$W_T \Delta y 2\alpha' \Delta z$ equals the net, time-average power-flux entering the closed surface S[1]. Since the time-average power flux entering S equals the average power dissipated inside S[2], then

$$W_T \Delta y 2\alpha' \Delta z = L = L_o + L_t \tag{4.2a}$$

where L_o is the average power dissipated due to the ohmic losses in the waveguide and L_t is the power extracted due to tunneling.

L can be separated into L_o and L_t because of the assumption $k_z \gg \alpha'$. Using this same argument,

$$\alpha' = \alpha + \alpha_t \tag{4.2b}$$

where α equals the attenuation due to ohmic losses and α_t equals the attenuation due to tunneling(attenuation due to the extraction of the energy from the waveguides through tunneling).

Separating the respective terms in eqns. (4.2a) and (4.2b),

$$W_T \Delta y 2\alpha_t \Delta z = L_t \tag{4.3a}$$

or

$$\alpha_t = \frac{L_t}{W_T \Delta y 2 \Delta z} \ . \tag{4.3b}$$

By definition,

---

1. Carl Johnk, *Engineering Electromagnetic Fields and Waves,* (New York: John Wiley & Sons, Inc., 1965), p. 419.
2. Ibid., p. 415.

$$L_t = \frac{1}{2}\int \bar{J}^* \cdot \overline{E_x}(\text{oxide})\,dr. \tag{4.4}$$

J is the current through the oxide due to tunneling. $\overline{E_x}$(oxide) is the electric field in the x direction across the oxide. dr is a volume element.

Since electrons tunnel in the x direction across the waveguide, the current flows in the x direction. Assuming that the electric field remains constant across the tunneling layer and J is constant with respect to the spatial coordinates, then

$$L_t = \frac{1}{2} J^* \overline{E_x}(\text{oxide})\Delta x \Delta y \Delta z = -\frac{J^* V}{2}\Delta y \Delta z. \tag{4.5}$$

where

$$V = -E_x(\text{oxide})\Delta x. \tag{4.6a}$$

and Δx is the oxide thickness.

Let σ' be defined as a tunneling conductivity that relates J to $\overline{E_x}$(oxide). Due to the nature of tunneling, σ' varies as $\overline{E_x}$(oxide) varies. By definition,

$$J = \sigma' E_x(\text{oxide}). \tag{4.6b}$$

Eqn. (4.5) now becomes

$$L_t = \sigma' \frac{|E_x(\text{oxide})|^2}{2}\Delta x \Delta y \Delta z. \tag{4.7}$$

Using equation (4.5), eqn. (4.3b) becomes

$$\alpha_t = -\frac{J^* V}{4W_T}. \tag{4.8}$$

From eqn. (4.6a),

$$\alpha_t = \frac{J^* E_x(\text{oxide})\Delta x}{4W_T}. \tag{4.9}$$

In this discussion, α_t will only be considered for the four layer waveguide.

4.3.1 α_t for the long range mode (TM_{00})

For the long range mode, $W_T \simeq W_{Td}$ and eqn (4.1a) becomes

$$W_{Td}=\int P_{zair}dx \tag{4.10}$$

where P_{zair} is P_z in the air layer.

Now P_{zair} is proportional to $|H_y|^2$ where H_y is given in equation (3.14b). Due to the boundary condition at $x=\infty$, $B_1=0$ in equation (3.14b) and

$$H_y=A_1e^{-jk_{xair}x} \tag{4.11}$$

where k_{xair} is k_x in the air layer. Eqn. (4.10) becomes

$$W_{Td}=\int_{i=0}^{i=\infty} P_z(0^+)e^{-2\alpha_{xair}x}dx \tag{4.12a}$$

which, when integrated is

$$W_{Td}=\frac{P_z(0^+)}{2\alpha_{xair}} \tag{4.12b}$$

where α_{xair} is the real part of $j(k_{xair})$. $P_z(0^+)$ is the Poynting vector in the z direction located on the air side of the air-metal interface.

Eqns. (3.19), (3.21) and (3.22) show that

$$P_z(0^+)=Re[\frac{E_x(0^+)H_y^*(0^+)}{2}] \tag{4.13}$$

and

$$P_z(0^+)=Re[\frac{\omega\epsilon_{air}}{k_z}]\frac{|E_x(0^+)|^2}{2}. \tag{4.14}$$

For the long range mode, $\epsilon_{air}=\epsilon_o$ and

$$k_z=\frac{\omega}{c}k_{znorm} \tag{4.15}$$

where k_{znorm} is the normalized or dimensionless wave number in the z direction. Since

$$c=\frac{1}{\sqrt{\epsilon_o\mu_o}},$$

eqn. (4.14) becomes

$$P_z(0^+)=\frac{|E_x(0^+)|^2}{2Re[k_{znorm}]}(\epsilon_o/\mu_o)^{1/2} \tag{4.16}$$

By definition,

$$\sqrt{(\mu_o/\epsilon_o)}=377\Omega,$$

so

$$P_z(0^+)=\frac{|E_x(0^+)|^2}{2(377\Omega)\mathrm{Re}[k_{znorm}]}. \tag{4.17}$$

Combining eqn. (4.17) with (4.12b),

$$W_{Td}=\frac{|E_x(0^+)|^2}{4(377\Omega)\mathrm{Re}[k_{znorm}]\alpha_{xair}}. \tag{4.18}$$

And placing eqn. (4.18) into (4.9),

$$\alpha_t=J^*E_x(\mathrm{oxide})\frac{\Delta x}{|E_x(0^+)|^2}(377\Omega)\mathrm{Re}[k_{znorm}]\alpha_{xair}. \tag{4.19}$$

4.3.2 α_t for the short range mode (TM_{10})

For the short range mode ($W_T \simeq W_{Td}$),

$$W_{Td}=\int P_z(\mathrm{oxide})dx. \tag{4.20}$$

From eqn. (3.21),

$$P_z(\mathrm{oxide})=\mathrm{Re}[\frac{\omega\epsilon_{ox}}{k_z}]\frac{|\overline{E_x}(\mathrm{oxide})|^2}{2.} \tag{4.21}$$

If the electric field across the oxide($\overline{E_x}$(oxide)) is constant, then P_z(oxide) is independent of x and

$$W_{Td}=P_z(\mathrm{oxide})\int dx=P_z(\mathrm{oxide})\Delta x. \tag{4.22}$$

Place eqn (4.22) into eqn (4.9), then

$$\alpha_t=\frac{J^*\overline{E_x}(\mathrm{oxide})\Delta x}{4P_z(\mathrm{oxide})\Delta x}. \tag{4.23}$$

Subsequently,

$$\alpha_t=\frac{J^*\overline{E_x}(\mathrm{oxide})(377\Omega)}{2|\overline{E_x}(\mathrm{oxide})|^2}\mathrm{Re}[\frac{k_{znorm}}{\epsilon_{rox}}] \tag{4.24}$$

where ϵ_{rox} is the relative permittivity of the oxide.

4.4 Calculation of J

Whiteley and Gustafson[3] have derived the equation for the inelastic tunnel current

$$J=\sum_n J_n^2\left(\frac{eV_r}{(h/2\pi)\omega}\right)\left[J\left(V_o+\frac{nh\omega}{2\pi e}\right)\right] \tag{4.25}$$

where $\left[J\left(V_o+\frac{nh\omega}{e2\pi}\right)\right]$ equals the elastic current at the bias potential $\left(V_o+\frac{nh\omega}{e2\pi}\right)$ and V_o is the applied bias voltage. J_n is the n^{th} order Bessel function of the first kind and h is Planck's constant.

For this solar cell,

$$V_r=-\overline{E_x}(\text{oxide})\Delta x \tag{4.26}$$

where Δx equals the width of the oxide.

The sum in n varies from $-\infty$ to $+\infty$. For a symmetric diode, $J = 0\frac{A}{m^2}$ because the current directed one way equals the current in the opposite direction.

α_t is calculated in section 4.5 for a symmetric diode. As a rough estimate for a non-symmetric diode, it is assumed that the summation in eqn. (4.25) is from $n = 0$ to $n = +\infty$. This assumption was used so we could find a non-zero value of α_t that could be compared to α.

4.5 Attenuation Due to Tunneling

In section 4.3 a procedure for calculating the attenuation due to tunneling for both modes of the four layer waveguide(air-silver-oxide-silver) was presented. This section presents the values of the attenuation calculated using this procedure. We have assumed $n_1=1.0$; $n_2=n_4=.06-j4.152$ and $n_3=1.5$. $f=4.86\text{x}10^{14}$ Hz. $d=150.\text{x}10^{-10}$m and $h=10.\text{x}10^{-10}$m. $E_x(\text{oxide})=5.\text{x}10^5\frac{\text{Volts}}{\text{cm}}$ and $J=31.25\frac{\text{Amps}}{\text{cm}^2}$ [4]. These values are representative of those which can be expected.

For the long range or TM_{00} mode ($E_x(0^+)\simeq 2E_x(\text{oxide})$),

$$\alpha_t=1.54\text{x}10^{-5}(\text{cm}^{-1}).$$

Comparing α_t with the α for the TM_{00} mode found in section 3.9,

---

3. S.R. Whiteley and T.K. Gustafson, "Stationary State Model for Normal Metal Tunnel Junction Phenomena," *IEEE Journal of Quantum Electronics*, QE-18 no. 9 (September 1982), pp. 1387-1398.

4. C.B. Duke, *Tunneling in Solids*, (New York: Academic Press, Inc., 1969), p. 62.

$$\frac{\alpha_t}{\alpha} = \frac{1.54\text{x}10^{-5}}{9.47\text{x}10^{1}} = 1.63\text{x}10^{-7} .$$

For the short range or TM_{10} mode, the coupling is much stronger and

$$\alpha_t = 1.5\text{x}10^{-2}(\text{cm}^{-1}).$$

Comparing α_t with the α for the TM_{10} mode found in section 3.9,

$$\frac{\alpha_t}{\alpha} = \frac{1.5\text{x}10^{-2}}{7.47\text{x}10^{4}} = 2.01\text{x}10^{-7} .$$

Thus we see that for both the TM_{00} and the TM_{10} modes, the attenuation due to tunneling (α_t) is too small for the solar cell to be operational in the ASOS waveguide. If this device is to be efficient α_t/α must be much larger than 1. Either α_t must be increased significantly or α must be reduced, or both.

4.6. Stacked Device

Two difficulties have been identified with using a tunnel diode structure for the conversion of solar energy into electrical energy. The first of these results from the fact that the presence of metal causes propagation losses. The second arises from the fact that the electromagnetic wave is weakly coupled into the tunnel structure, and hence the absorption coefficient due to tunneling is quite small. The reason for the latter is apparent if we consult Fig. 4.5a in which it is seen that when most of the energy is stored in a region external to the tunnel structure, the coupling between the energy propagating in the structure and the tunneling process is very weak. When most of the energy is stored in the tunnel region (Figure 4.5b) the absorption coefficient is 3 orders of magnitude larger. However, in this case the propagation losses are also 3 orders of magnitude higher. One possible solution to this problem is to use the structure shown in Fig. 4.6, in which a series of tunnel structures is stacked one upon another, such that the thickness of the total structure approaches the thickness of the region in which the energy is stored. A much stronger coupling would be expected between the electromagnetic wave and this stacked structure. In addition, wherever possible, the metal of the structure is replaced by a semiconductor, thus reducing the propagation losses in this structure.

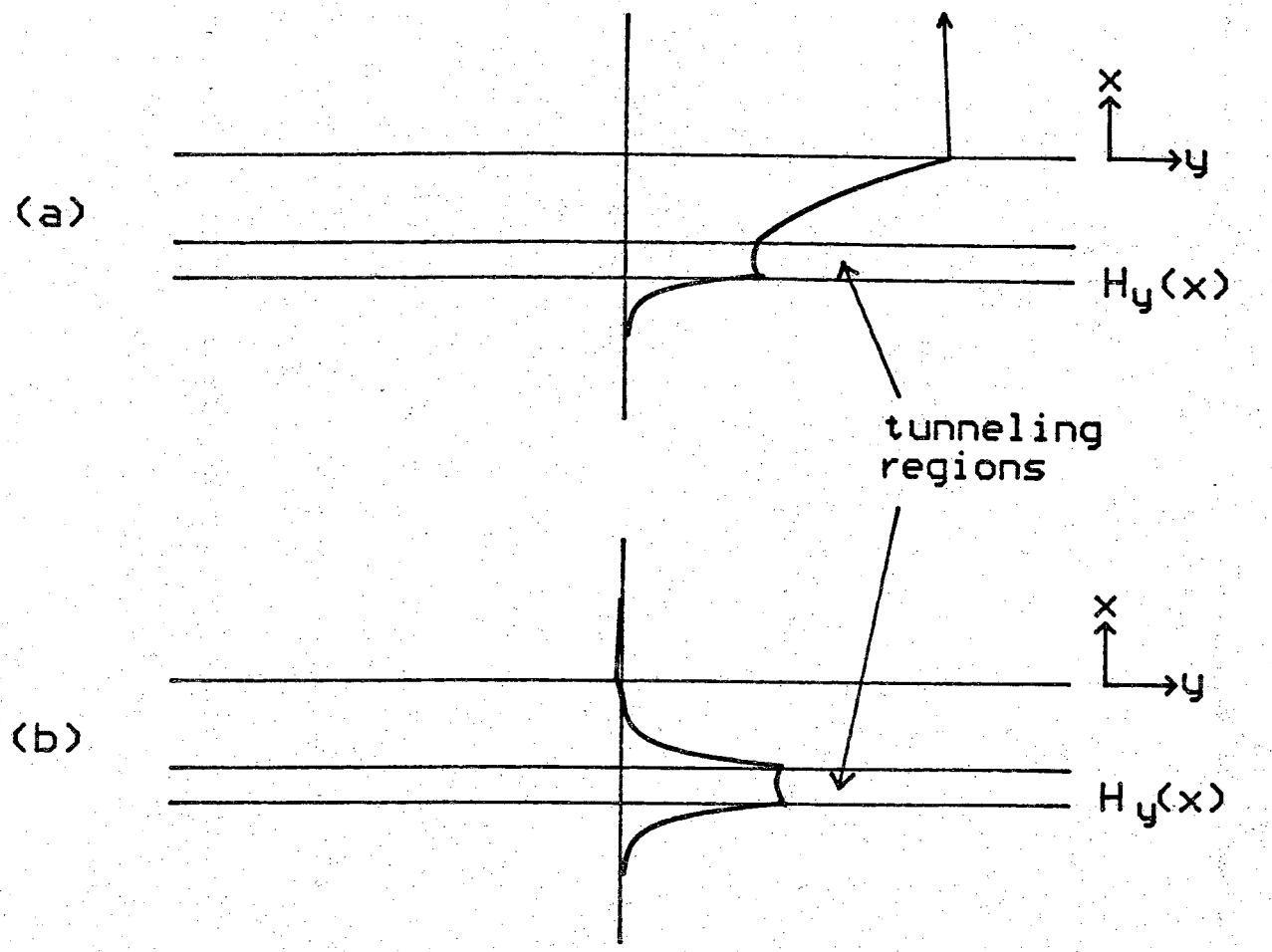

Figure 4.5. (a) The long range mode (very weak coupling) and (b) the short range mode (stronger coupling than in (a)) of the four layer waveguide.

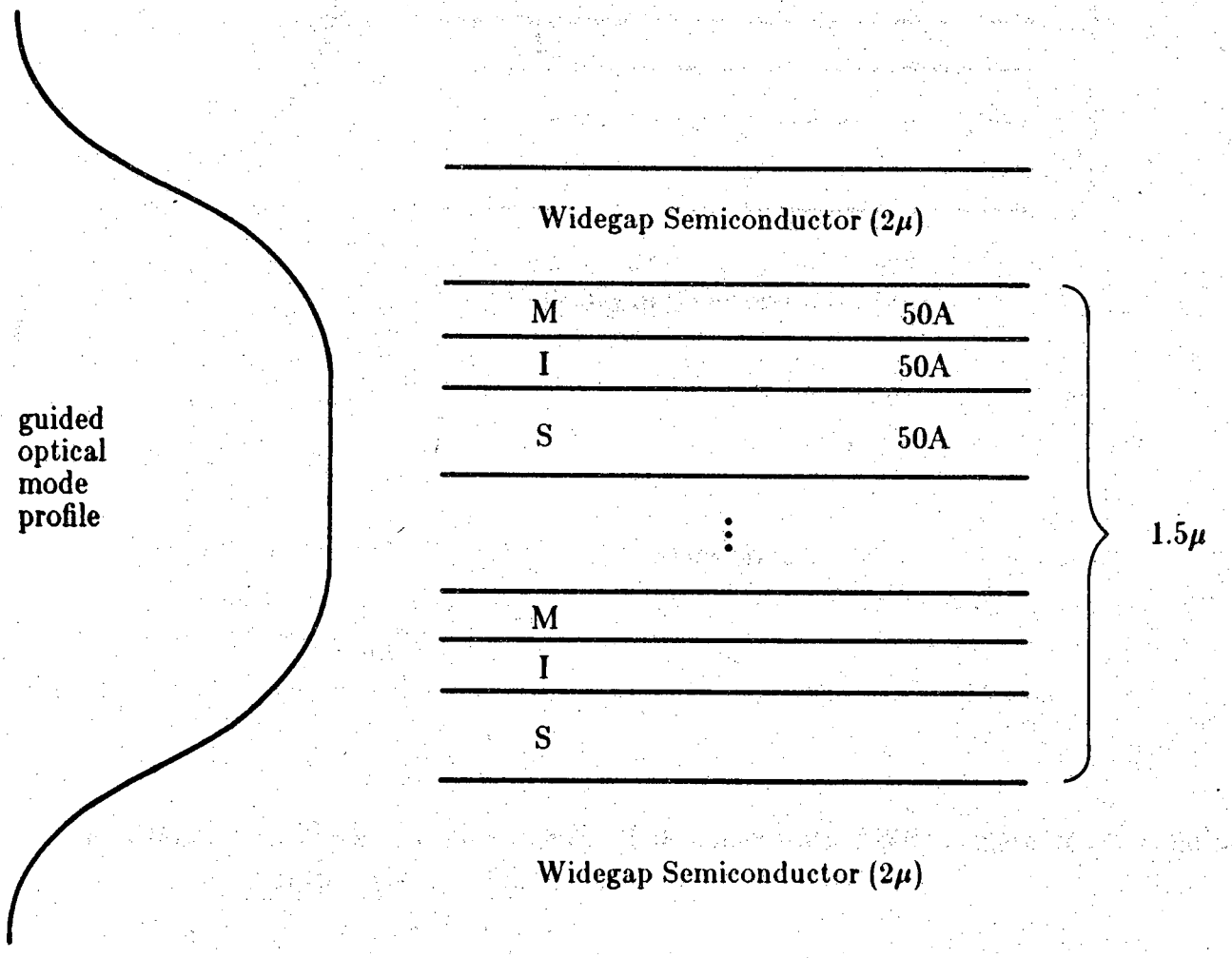

Figure 4.6. A stack of tunnel diodes. This configuration should increase the coupling to the electromagnetic wave.

5. Conclusions and Implications for Future Work

Results obtained to date indicate the following:

1. Metal-insulator-metal tunnel structures do not contain sufficient asymmetry in their properties to allow efficient conversion of solar energy. Structures required will be either metal-insulator-semiconductor structures or semiconductor-insulator-semiconductor structures.
2. It is useful to take a general view of the guided waves and not confine consideration to surface plasmons.
3. Even if mode conversion between a surface plasmon and a tunnel mode plasmon can be efficiently accomplished, the coupling between the tunnel mode plasmon and tunneling is sufficiently weak that most of the energy is lost in propagation losses and is not converted to useful energy.
4. If the proper materials can be found such that the strong coupling into photon aided tunneling can occur, a cascaded tunnel diode structure appears to be promising for broadband energy conversion.
5. The tunnel diode has many of the characteristics that one would attribute to an electronically tunable bandgap in a conventional solar cell.
6. A stack of tunnel diodes may be a promising way of obtaining more efficient coupling into a guided wave.
7. At this point, a critical problem would appear to be the determination of whether or not it is possible to obtain strong enough coupling of the photons into tunneling process to make the energy conversion scheme feasible.
8. We should remove as much metal from the structure as possible.

LIST OF REFERENCES

Lynn Anderson, "Harnessing Surface Plasmons for Solar Energy Conversion," *Proceedings of the SPIE - The International Society for Optical Engineering,* **408,** (1983), pp. 172-178.

Lynn Anderson, Proceedings 16th I.E.E.E. Photovoltaic Specialists Conference, (1982), pp. 371-377.

Lynn Anderson, Proceedings 17th Intersociety Energy Conversion Engineering Conference, (1982), pp. 125-130.

Ruel Churchill and James Brown, *Complex Variables and Applications,* 3rd ed., (New York: Mcgraw Hill, Inc., 1984).

L.C. Davis, "Theory of Surface-Plasmon Excitation in Metal-Insulator-Metal Tunnel Junctions," *Physical Review B,* **16,** no. 6 (15 September, 1977), pp. 2482-2490.

A.H. Dayem and R.J. Martin, "Quantum Interaction of Microwave Radiation with Tunneling between Superconductors," *Physical Review Letters* **8,** no. 6 (15 March, 1962), pp. 246-248.

C.B. Duke, *Tunneling in Solids,* (New York: Academic Press, Inc., 1969).

E.N. Economou, "Surface Plasmons in Thin Films" *Physical Review,* **182,** no. 2 (10 June, 1969), pp. 539-554.

M. Fukui, V.C.Y. So and R. Normandin, "Lifetimes of Surface Plasmons in Thin Silver Films," *Physica Status Solidi (b),* **91,** (1979), pp. k61-k64.

Gmelin Handbuch - Der Anorganischen Chemie, Ed. R.J. Meyer and E.H. Pietsch, (Berlin: Verlag Chemie).

Martin Green, *Solar Cells,* (Englewood Cliffs, N.J.: Prentice Hall, Inc., 1982).

T.K. Gustafson, "Coherent Conversion of the Sunlight Spectrum," NASA Grant NAG 3-88, July, 1980 - April, 1982.

R.C. Jaklevic and J. Lambe, "Molecular Vibration Spectra by Electron Tunneling," *Physical Review Letters,* **17,** no. 22 (28 November, 1966) pp. 1139-1140.

Carl Johnk, *Engineering Electromagnetic Fields and Waves,* (New York: John Wiley & Sons, Inc., 1965).

P.B Johnson and R.W. Christy, "Optical Constants of the Noble Metals," *Physical Review B,* **6,** no. 12 (15 December, 1972), pp. 4370-4379.

Edward Jordan and Keith Balmain, *Electromagnetic Waves and Radiation Systems,* (Englewood Cliffs, N.J.: Prentice Hall, Inc., 1968).

John Lambe and S.L. McCarthy, "Light Emission from Inelastic Electron Tunneling," *Physical Review Letters,* **37,** no. 14 (4 October, 1976), pp. 923-925.

Dietrich Marcuse, *Theory of Dielectric Optical Waveguides,* (New York: Academic Press, 1974).

Simon Ramo, John Whinnery and Theodore Van Duzer, *Fields and Waves in Communications Electronics,* (New York: John Wiley & Sons, Inc., 1965).

Dror Sarid, "Long Range Surface-Plasma Waves on Very Thin Metal Films," *Physical Review Letters,* **47,** no. 26 (28 December, 1981), pp. 1927-1929.

D.J. Scalapino and S.M. Marcus, "Theory of Inelastic Electron-Molecule Interaction in Tunnel Junctions," *Physical Review Letters,* **18,** no. 12 (20 March, 1967), pp. 459-461.

J. Schoenwald, E. Burstein and J.M. Elson, "Propagation of Surface Polaritons over Macroscopic Distances at Optical Frequencies," *Solid State Communications,* **12,** no. 3 (1973), pp. 185-189.

L.G. Schulz, "The Optical Constants of Silver, Gold, Copper and Aluminum. I. The Absorption Coefficient *k.* II. The index of refraction *n, Journal of the Optical Society of America,* **44,** no. 5 (May, 1954), pp. 357-368.

Peter Stark, *Introduction to Numerical Methods,* (New York: The Macmillan Company, 1970).

G.I. Stegeman and J.J. Burke, "Long Range Surface Plasmons in Electrode Structures," *Applied Physics Letters,* **43,** no. 3 (1 August, 1983), pp. 222-223.

W. Steinmann, "Optical Plasma Resonances in Solids," *Physica Status Solidi,* **28,** (1968), pp. 437-462.

P.K. Tien and J.P. Gordon, "Multiphoton Process Observed in the Interaction of Microwave Fields with the Tunneling between Superconductor Films," *Physical Review,* **129,** no. 2 (15 January, 1963), pp. 647-651.

P.K. Tien and R. Ulrich, "Theory of Prism-Film Coupler and Thin-Film Light Guides," *Journal of the Optical Society of America,* **60,** no. 10 (October, 1970), pp. 1325-1337.

S.R. Whiteley and T.K. Gustafson, "Stationary State Model for Normal Metal Tunnel Junction Phenomena," *IEEE Journal of Quantum Electronics,* **QE-18,** no. 9 (September, 1982), pp. 1387-1398.

Appendix A

As discussed in section 3.2, a method exists by which the dispersion relationship can be obtained for parallel plate waveguides. This appendix demonstrates how to use this method for a four layer waveguide.

Since the modes of interest for the solar cell are TM modes, only the dispersion relationship for the TM modes will be calculated.

An example of a four layer waveguide is presented in Fig. 3.7.

The magnetic fields in each of the layers can be represented as

$$H_{1y}=B_1e^{-j\psi x} \qquad \text{layer 1} \qquad \text{(A.1a)}$$

$$H_{2y}=A_2e^{j\varsigma x}+B_2e^{-j\varsigma(x+d)} \qquad \text{layer 2} \qquad \text{(A.1b)}$$

$$H_{3y}=A_3e^{j\kappa(x+d)}+B_3e^{-j\kappa(x+d+h)} \qquad \text{layer 3} \qquad \text{(A.1c)}$$

$$H_{4y}=A_4e^{j\gamma(x+d+h)} \qquad \text{layer 4} \qquad \text{(A.1d)}$$

where

$$\psi=\sqrt{n_1^2\left(\frac{\omega}{c}\right)^2-k_z^2} \qquad \text{(A.2a)}$$

$$\varsigma=\sqrt{n_2^2\left(\frac{\omega}{c}\right)^2-k_z^2} \qquad \text{(A.2b)}$$

$$\kappa=\sqrt{n_3^2\left(\frac{\omega}{c}\right)^2-k_z^2} \qquad \text{(A.2c)}$$

$$\gamma=\sqrt{n_4^2\left(\frac{\omega}{c}\right)^2-k_z^2}\,. \qquad \text{(A.2d)}$$

For the TM mode,

$$E_z=\frac{-j}{\epsilon\omega}\left(\frac{\partial H_y}{\partial x}\right)$$

and consequently, the E_z fields in the four layers are

$$E_{1z}=\frac{-j}{\epsilon_1\omega}\,-j\psi B_1 e^{-j\psi x} \tag{A.3a}$$

$$E_{2z}=\frac{-j}{\epsilon_2\omega}\,-j\varsigma[-A_2 e^{j\varsigma x}+B_2 e^{-j\varsigma(x+d)}] \tag{A.3b}$$

$$E_{3z}=\frac{-j}{\epsilon_3\omega}\,-j\kappa[-A_3 e^{j\kappa(x+d)}+B_3 e^{-j\kappa(x+d+h)}] \tag{A.3c}$$

$$E_{4z}=\frac{-j}{\epsilon_4\omega}\,-j\gamma[-A_4 e^{j\gamma(x+d)}]\ . \tag{A.3d}$$

The boundary condition of Maxwell's eqns. state that the tangential magnetic and tangential electric fields are continuous across the layer interfaces.

At x=0, or the interface between layers 1 and 2,

$$H_{1y}=H_{2y} \tag{A.4a}$$

$$E_{1z}=E_{2z}\ . \tag{A.4b}$$

Therefore,

$$B_1=A_2+B_2 e^{-j\varsigma d} \tag{A.5a}$$

$$\frac{\psi}{\epsilon_1}B_1=\frac{\varsigma}{\epsilon_2}(-A_2+B_2 e^{-j\varsigma d})\ . \tag{A.5b}$$

From eqns. (A.5a) and (A.5b), we obtain

$$A_2=\frac{B_1}{2}\left(1-\frac{\psi\epsilon_2}{\varsigma\epsilon_1}\right) \tag{A.6a}$$

$$B_2=\frac{B_1}{2}\left(1+\frac{\psi\epsilon_2}{\varsigma\epsilon_1}\right)e^{j\varsigma d}. \tag{A.6b}$$

At x=-d, or the interface between layers 2 and 3,

$$H_{2y}=H_{3y} \tag{A.7a}$$

$$E_{2z}=E_{3z}\,. \tag{A.7b}$$

Therefore,

$$A_2e^{-j\varsigma d}+B_2=A_3+B_3e^{-j\kappa h} \tag{A.8a}$$

$$\frac{\varsigma}{\epsilon_2}[-A_2e^{-j\varsigma d}+B_2]=\frac{\kappa}{\epsilon_3}[-A_3+B_3e^{-j\kappa h}]. \tag{A.8b}$$

At $x=-(d+h)$, or the interface between layers 3 and 4,

$$H_{3y}=H_{4y} \tag{A.9a}$$

$$E_{3z}=E_{4z}\,. \tag{A.9b}$$

Therefore,

$$A_3e^{-j\kappa h}+B_3=A_4 \tag{A.10a}$$

$$\frac{\kappa}{\epsilon_3}[-A_3e^{-j\kappa h}+B_3]=-A_4\frac{\gamma}{\epsilon_4}. \tag{A.10b}$$

From eqns. (A.10a) and (A.10b),

$$A_3=\frac{A_4}{2}(1+\frac{\gamma\epsilon_3}{\kappa\epsilon_4})e^{j\kappa h} \tag{A.11a}$$

$$B_3=\frac{A_4}{2}(1-\frac{\gamma\epsilon_3}{\kappa\epsilon_4})\,. \tag{A.11b}$$

Placing eqns. (A.6) and (A.11) into eqns. (A.8), we obtain

$$\frac{B_1}{2}(1-\frac{\psi\epsilon_2}{\varsigma\epsilon_1})e^{-j\varsigma d}+\frac{B_1}{2}(1+\frac{\psi\epsilon_2}{\varsigma\epsilon_1})e^{j\varsigma d}=$$

$$\frac{A_4}{2}(1+\frac{\gamma\epsilon_3}{\kappa\epsilon_4})e^{j\kappa h}+\frac{A_4}{2}(1-\frac{\gamma\epsilon_3}{\kappa\epsilon_4})e^{-j\kappa h} \tag{A.12a}$$

$$\frac{\varsigma}{\epsilon_2}\frac{B_1}{2}[(1+\frac{\psi\epsilon_2}{\varsigma\epsilon_1})e^{j\varsigma d}-(1-\frac{\psi\epsilon_2}{\varsigma\epsilon_1})e^{-j\varsigma d}]=$$

$$\frac{\kappa}{\epsilon_3}\frac{A_4}{2}[(1-\frac{\gamma\epsilon_3}{\kappa\epsilon_4})e^{-j\kappa h}-(1+\frac{\gamma\epsilon_3}{\kappa\epsilon_4})e^{j\kappa h}] . \qquad \text{(A.12b)}$$

Combining the exponents, eqns. (A.12) become

$$B_1[\cosh(j\varsigma d)+\frac{\psi\epsilon_2}{\varsigma\epsilon_1}\sinh(j\varsigma d)]=$$

$$A_4[\cosh(j\kappa h)+\frac{\gamma\epsilon_3}{\kappa\epsilon_4}\sinh(j\kappa h)] \qquad \text{(A.13a)}$$

$$\frac{\varsigma}{\epsilon_2}B_1[\sinh(j\varsigma d)+\frac{\psi\epsilon_2}{\varsigma\epsilon_1}\cosh(j\varsigma d)]=$$

$$\frac{\kappa}{\epsilon_3}A_4[-\sinh(j\kappa h)-\frac{\gamma\epsilon_3}{\kappa\epsilon_4}\cosh(j\kappa h)] . \qquad \text{(A.13b)}$$

Solving for B_1/A_4 from eqns. (A.13),

$$\frac{B_1}{A_4}=\frac{\cosh(j\kappa h)+\frac{\gamma\epsilon_3}{\kappa\epsilon_4}\sinh(j\kappa h)}{\cosh(j\varsigma d)+\frac{\psi\epsilon_2}{\varsigma\epsilon_1}\sinh(j\varsigma d)} \qquad \text{(A.14a)}$$

and

$$\frac{B_1}{A_4}=\frac{\kappa\epsilon_2}{\varsigma\epsilon_3}[\frac{-\sinh(j\kappa h)-\frac{\gamma\epsilon_3}{\kappa\epsilon_4}\cosh(j\kappa h)}{\sinh(j\varsigma d)+\frac{\psi\epsilon_2}{\varsigma\epsilon_1}\cosh(j\varsigma d)}] . \qquad \text{(A.14b)}$$

The right hand sides of eqns. (A.14a) and (A.14b) equal each other and we obtain

$$\frac{1+\frac{\gamma\epsilon_3}{\kappa\epsilon_4}\tanh(j\kappa h)}{1+\frac{\psi\epsilon_2}{\varsigma\epsilon_1}\tanh(j\varsigma d)}=\frac{\kappa\epsilon_2}{\varsigma\epsilon_3}[\frac{-\tanh(j\kappa h)-\frac{\gamma\epsilon_3}{\kappa\epsilon_4}}{\tanh(j\varsigma d)+\frac{\psi\epsilon_2}{\varsigma\epsilon_1}}]. \qquad \text{(A.15)}$$

Multiply both sides of eqn (A.15) by $\frac{\varsigma\epsilon_3}{\kappa\epsilon_2}[\tanh(j\varsigma d)+\frac{\psi\epsilon_2}{\varsigma\epsilon_1}]$ and

$$(1+\frac{\gamma\epsilon_3}{\kappa\epsilon_4}\tanh(j\kappa h))[\frac{\varsigma\epsilon_3}{\kappa\epsilon_2}\frac{(\tanh(j\varsigma d)+\frac{\psi\epsilon_2}{\varsigma\epsilon_1})}{1+\frac{\psi\epsilon_2}{\varsigma\epsilon_1}\tanh(j\varsigma d)}] =$$

$$-\tanh(j\kappa h)-\frac{\gamma\epsilon_3}{\kappa\epsilon_4}. \qquad \text{(A.16)}$$

Now let

$$\xi=[\frac{\varsigma\epsilon_3}{\kappa\epsilon_2}(\frac{\tanh(j\varsigma d)+\frac{\psi\epsilon_2}{\varsigma\epsilon_1}}{1+\frac{\psi\epsilon_2}{\varsigma\epsilon_1}\tanh(j\varsigma d)})] \qquad \text{(A.17)}$$

then

$$(1+\frac{\gamma\epsilon_3}{\kappa\epsilon_4}\tanh(j\kappa h))\xi = -\tanh(j\kappa h)-\frac{\gamma\epsilon_3}{\kappa\epsilon_4} \qquad \text{(A.18a)}$$

or in another form,

$$\tanh(j\kappa h)(1+\frac{\gamma\epsilon_3}{\kappa\epsilon_4}\xi) = -\frac{\gamma\epsilon_3}{\kappa\epsilon_4}-\xi\,. \qquad \text{(A.18b)}$$

From eqn. (A.18b),

$$\tanh(j\kappa h) = \frac{-\frac{\gamma\epsilon_3}{\kappa\epsilon_4}-\xi}{1+\frac{\gamma\epsilon_3}{\kappa\epsilon_4}\xi}\,. \qquad \text{(A.19)}$$

By definition,

$$\tanh(j\kappa h)=j\tan\kappa h \qquad \text{(A.20a)}$$

and

$$\tanh(j\varsigma d)=j\tan\varsigma d. \qquad \text{(A.20b)}$$

Letting

$$\psi=j\psi_1 \qquad \text{(A.21a)}$$

and

$$\gamma = j\gamma_1, \tag{A.21b}$$

ξ becomes

$$\xi = \left[\frac{j\varsigma\epsilon_3}{\kappa\epsilon_2}\,\frac{\left(\tanh(j\varsigma d) + \frac{\psi_1\epsilon_2}{\varsigma\epsilon_1}\right)}{1 - \frac{\psi_1\epsilon_2}{\varsigma\epsilon_1}\tanh(j\varsigma d)}\right] = j\xi_1. \tag{A.21c}$$

Combining the results of eqns. (A.20) and (A.21) into eqn. (A.19),

$$j\tan\kappa h = \frac{\frac{-j\gamma_1\epsilon_3}{\kappa\epsilon_4} - j\xi_1}{1 + \frac{j\gamma_1\epsilon_3}{\kappa\epsilon_4} j\xi_1}. \tag{A.22}$$

Dividing by j,

$$\tan\kappa h = \frac{\frac{-\gamma_1\epsilon_3}{\kappa\epsilon_4} - \xi_1}{1 - \frac{\gamma_1\epsilon_3}{\kappa\epsilon_4}\xi_1}. \tag{A.23}$$

This is the dispersion relationship for the four layer waveguide.

Everything in eqn. (A.23) depends upon the dielectric constants and the thicknesses of the layers and upon ψ, ς, κ, γ which are found from eqns. (A.2). In eqns. (A.2), ψ, ς, κ, γ depend only on two variables - k_z and ω. If ω is fixed, both sides of eqn. (A.23) depend only on k_z. One solves the eqn. by choosing the correct value of k_z.

Appendix B

This appendix presents the Newton Raphson method used to solve for the zeroes of an equation.

For real numbers, the eqn. of the Newton Raphson method is[1]

$$b_{n+1} = b_n - \frac{f(b_n)}{f'(b_n)} \tag{B.1}$$

where f is the function that goes to zero, f' is the derivative with respect to b of f. Eqn. (B.1) comes about because of the definition of f'.

$$f' = \frac{df}{db} = \frac{f(b_{n+1})-f(b_n)}{b_{n+1}-b_n} \tag{B.2}$$

Figure B.1 describes pictorially how the Newton Raphson method works. At $x=b_{n+1}$, $f(b_{n+1})=0$. Due to this fact, eqn. (B.2) readily transforms into eqn. (B.1).

Now if the b's are complex numbers, then let

$$b = x + jy, \tag{B.3a}$$

$$f = u + jv, \tag{B.3b}$$

and[2]

$$f' = u_x + jv_x. \tag{B.3c}$$

Where by definition,

$$u_x = \frac{\partial u}{\partial x} \tag{B.4a}$$

and

$$v_x = \frac{\partial v}{\partial x}. \tag{B.4b}$$

Also,

$$u_y = \frac{\partial u}{\partial y} \tag{B.4c}$$

and

---

1. Peter Stark, *Introduction to Numerical Methods* (New York: The Macmillan Company, 1970), pp. 85-89.
2. Ruel Churchill and James Brown, *Complex Variables and Applications*, 3rd ed., (New York: McGraw Hill, Inc., 1984), pp. 43-47.

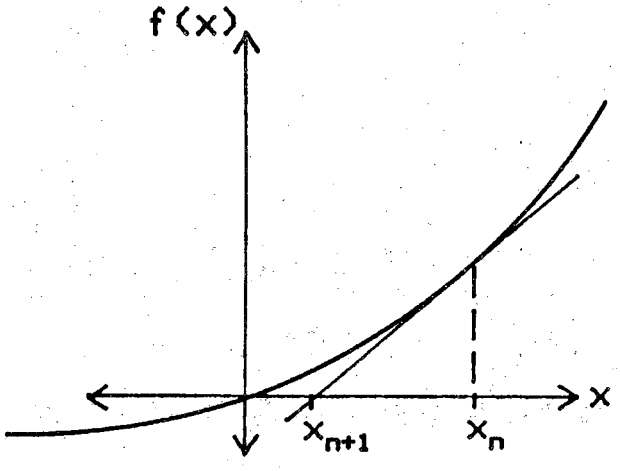

Figure B.1. Newton Raphson method applied to f(x).

$$v_y = \frac{\partial v}{\partial y}. \tag{B.4d}$$

Based upon eqns. (B.3) and (B.4),

$$\frac{f}{f'} = \frac{(u+jv)}{(u_x+jv_x)}\left[\frac{(u_x-jv_x)}{(u_x-jv_x)}\right]. \tag{B.5a}$$

$$\frac{f}{f'} = \frac{uu_x+vv_x+j(vu_x-uv_x)}{u_x^2+v_x^2}. \tag{B.5b}$$

The Cauchy Riemann equations state [3]

$$u_x = v_y \tag{B.6a}$$

and

$$u_y = -v_x. \tag{B.6b}$$

Placing these conditions into eqn. (B.5b),

$$\frac{f(b_n)}{f'(b_n)} = \left[\frac{uu_x+vu_y+j(vu_x+uu_y)}{u_x^2+u_y^2}\right]_{x_n,y_n}. \tag{B.7}$$

For complex numbers, eqn. (B.1) becomes

$$x_{n+1}+jy_{n+1} = x_n+jy_n-\left[\frac{uu_x+vu_y+j(vu_x+uu_y)}{u_x^2+u_y^2}\right]_{x_n,y_n}. \tag{B.8}$$

where the subscripts (x_n, y_n) denote that eqn. (B.7) is evaluated at (x_n, y_n).

Eqn. (B.8) separates into two equations.

$$x_{n+1} = x_n+\left[\frac{-uu_x+vu_y}{u_x^2+u_y^2}\right]_{x_n,y_n} \tag{B.9a}$$

$$y_{n+1} = y_n-\left[\frac{-vu_x+uu_y}{u_x^2+u_y^2}\right]_{x_n,y_n}. \tag{B.9b}$$

These eqns. comprise the Newton Raphson method for complex numbers.

Pick a number ϵ which is small enough so that when

$$\epsilon > |x_{n+1}-x_n| \tag{B.10a}$$

and

---

3. Ibid., p. 45.

$$\epsilon > |y_{n+1} - y_n| , \tag{B.10a}$$

then the approximate zero $f(b_{n+1})$ is sufficiently close to the actual zero.

Appendix C

Most of the eqns. needed to solve H_y are in appendix A. Using these eqns, this appendix offers a method that finds H_y for a four layer parallel plate waveguide. The procedure remains the same for parallel plate waveguides with any number of layers.

One solves for H_y by simply finding the constants B_1, A_2, B_2, A_3, B_3, A_4.

Pick a number for B_1 or A_4 in eqns. (A.1). For example, $B_1 = 2.(\frac{\text{Amps}}{\text{m}})$.

A_2 and B_2 are found from eqns. (A.6a) and (A.6b) respectively.

Using the values of A_2 and B_2 , eqns. (A.8a) and (A.8b) calculate the values of A_3 and B_3 .

Then use eqn. (A.10a) or (A.10b) to calculate the value of A_4.

Now that the constants B_1, A_2, B_2, A_3, B_3, A_4 are known, use eqns. (A.1) to solve for H_y over the whole range in the x direction.

For the electric fields, use eqns. (A.3) to calculate $E_z(x)$. E_x only differs from H_y by a constant and can be obtained through the use of eqn. (3.13a).